



PAPER • OPEN ACCESS

Symmetry breaking and the geometry of reduced density matrices

To cite this article: V Zauner *et al* 2016 *New J. Phys.* **18** 113033

View the [article online](#) for updates and enhancements.

You may also like

- [Delay-induced dynamics and jitter reduction of passively mode-locked semiconductor lasers subject to optical feedback](#)

C Otto, K Lüdge, A G Vladimirov *et al.*

- [Outrit squeezing via semiclassical evolution](#)

Andrei B Klimov, Hossein Tavakoli Dinani, Zachari E D Medendorp *et al.*

- [Phase diagram of three dimensional disordered nodal-line semimetals: weak localization to Anderson localization](#)

K X Jia, X Y Liu, R Ma *et al.*



PAPER

Symmetry breaking and the geometry of reduced density matrices

OPEN ACCESS

RECEIVED
29 June 2016ACCEPTED FOR PUBLICATION
24 October 2016PUBLISHED
17 November 2016V Zauner¹, D Draxler¹, L Vanderstraeten², J Haegeman² and F Verstraete^{1,2}¹ Vienna Center for Quantum Technology, University of Vienna, Boltzmannngasse 5, A-1090 Wien, Austria² Ghent University, Krijgslaan 281, B-9000 Gent, BelgiumE-mail: valentin.zauner@univie.ac.at**Keywords:** strongly correlated systems, phase transitions, symmetry breaking, convex sets, thermodynamic surfaces, tensor network states

Original content from this work may be used under the terms of the [Creative Commons Attribution 3.0 licence](https://creativecommons.org/licenses/by/4.0/).

Any further distribution of this work must maintain attribution to the author(s) and the title of the work, journal citation and DOI.

**Abstract**

The concept of symmetry breaking and the emergence of corresponding local order parameters constitute the pillars of modern day many body physics. We demonstrate that the existence of symmetry breaking is a consequence of the geometric structure of the convex set of reduced density matrices of all possible many body wavefunctions. The surfaces of these convex bodies exhibit non-analyticities, which signal the emergence of symmetry breaking and of an associated order parameter and also show different characteristics for different types of phase transitions. We illustrate this with three paradigmatic examples of many body systems exhibiting symmetry breaking: the quantum Ising model, the classical q -state Potts model in two-dimensions at finite temperature and the ideal Bose gas in three-dimensions at finite temperature. This state based viewpoint on phase transitions provides a unique novel tool for studying exotic many body phenomena in quantum and classical systems.

1. Introduction

In a series of ground breaking papers in the late 19th century, Gibbs [1–3] elegantly derived the thermodynamic stable state of a given substance through the minimization of some thermodynamic potential (later known as the free energy), in fact by means of a geometric construction. In particular, Gibbs considered a surface given by the possible values of the thermodynamic extensive quantities (such as e.g. energy, volume and entropy) of a system of interest and realized that points on this surface with tangent planes of equal orientation correspond to possible stable states of the substance at a temperature and pressure given by the orientation of the tangent plane. If two (or more) points belong to the same tangent plane, the corresponding states can coexist in equilibrium, characteristic for first order phase transitions. If two or more points have tangent planes with equal orientation but different distance to the origin, the state whose tangent plane is closer to the origin is metastable, corresponding to a supercritical system [3].

This geometrical construction can be interpreted as identifying the thermodynamically stable states as the extreme points of a convex set consisting of all possible realizable values of the thermodynamic extensive quantities of a given system. In the case of Gibbs' construction the relevant convex set is essentially the convex hull of the thermodynamic surface, termed 'secondary surface' by Maxwell (who also produced a plaster clay model of the surface for water as a present to Gibbs in 1874). All thermodynamic properties of a system of interest can then be read off from the geometric features of this set and phase transitions correspond to non-analyticities on the surface, which arise by considering convex hulls of analytic functions [4].

While Gibbs' original construction is capable of detecting regions of phase coexistence at first order phase transitions, they however show no signatures at second order phase transitions, as there the thermodynamic extensive quantities vary continuously across the critical point. In this work we demonstrate that by including the order parameter corresponding to such a phase transition as an extensive quantity into these sets, phase transitions are signaled through the appearance of characteristic geometrical features in the form of ruled surfaces. As these sets exist as a collection of all possible realizable states of a given system without any prior reference to any Hamiltonian which generates dynamics, the reason for the occurrence of symmetry breaking phase transitions thus lies in the geometry of the space of all possible realizable states.

We show the generality of this geometric interpretation by explicitly extending Gibbs' construction to quantum and classical lattice spin models, as well as quantum field theories. Our work considerably extends and clarifies the convex set picture in the context of the N -representability problem in quantum chemistry [5–8], and provides a very nice connection to the discussions on the monogamy of entanglement and mean-field theory in [9].

2. Convex sets for quantum lattice systems

Ground states of quantum many body Hamiltonians composed of local interactions are very special: in order to minimize the energy expectation value they have extremal local correlations, but those correlations must be compatible with the global symmetry of the many body Hamiltonian such as translation invariance. The competition between those two requirements is responsible for the emergence of the typical long-range properties as exhibited in strongly correlated materials. This is best illustrated by the $S = 1/2$ Heisenberg quantum antiferromagnet: the energy density would be minimized if all nearest neighbor reduced density matrices (RDMs) were singlets, but due to the monogamy properties of entanglement [10, 11], this is not compatible with the translation invariance of the ground state. Hence the symmetry requirements smear the entanglement out into a globally entangled state with algebraically decaying correlations and (quasi) long range order.

This competition is nicely reflected in the convex set of the RDMs of all possible pure and mixed quantum many body states of the entire system³.

Let us for example consider a lattice of spin-1/2 quantum systems and arbitrary spatial dimension d , take random quantum states ρ_α , and make a scatter plot of the expectation values $\langle Z \rangle \equiv \frac{1}{N} \text{Tr}(\rho_\alpha \sum_i Z_i)$ and $\langle X \otimes X \rangle \equiv \frac{2}{NK} \text{Tr}(\rho_\alpha \sum_{\langle ij \rangle} X_i X_j)$, where X and Z are Pauli matrices, N is the number of sites, K is the coordination number of the lattice and the sum is over nearest neighbors only. This is equivalent to restricting to translation invariant states ρ_α^{TI} and measuring the 1 or 2-site observables Z and $X \otimes X$, for which only the 2-site RDM is needed. As these terms do not commute, a large expectation value $\langle X \otimes X \rangle$ will lead to a small expectation value $\langle Z \rangle$, giving rise to a curved boundary of the generated set. Due to the convexity of the set of 2-site RDMs, the generated body is also convex and corresponds to a two-dimensional projection of the full 15-dimensional set of all possible 2-site RDMs. The extreme points of this set correspond to ground states of a family of quantum Ising Hamiltonians of the form

$$H = -\frac{2J}{K} \sum_{\langle ij \rangle} X_i X_j - B_z \sum_i Z_i. \quad (1)$$

Indeed, surfaces of constant energy are represented by lines $E = -J \langle X \otimes X \rangle - B_z \langle Z \rangle$ in this plot, where the orientation of these lines is given by the parameters J, B_z and their distance to the origin is proportional to (minus) the energy. Hence the expectation values of the states with minimal energy must correspond to extreme points for which the lines are tangent to the convex set and thus at maximum distance from the origin, or equivalently, every point on the boundary of the generated set corresponds to the ground state of (1) with parameters given by the orientation of the tangent line through that point.

The situation becomes much more interesting and the presence of symmetry breaking becomes immediately evident when adding an extra axis corresponding to the expectation value of $\langle X \rangle \equiv \frac{1}{N} \text{Tr}(\rho_\alpha \sum_i X_i)$ to the scatter plot. The extreme points of the resulting convex set now correspond to ground states of the quantum Ising model including a longitudinal field which explicitly breaks the \mathbb{Z}_2 spin flip symmetry

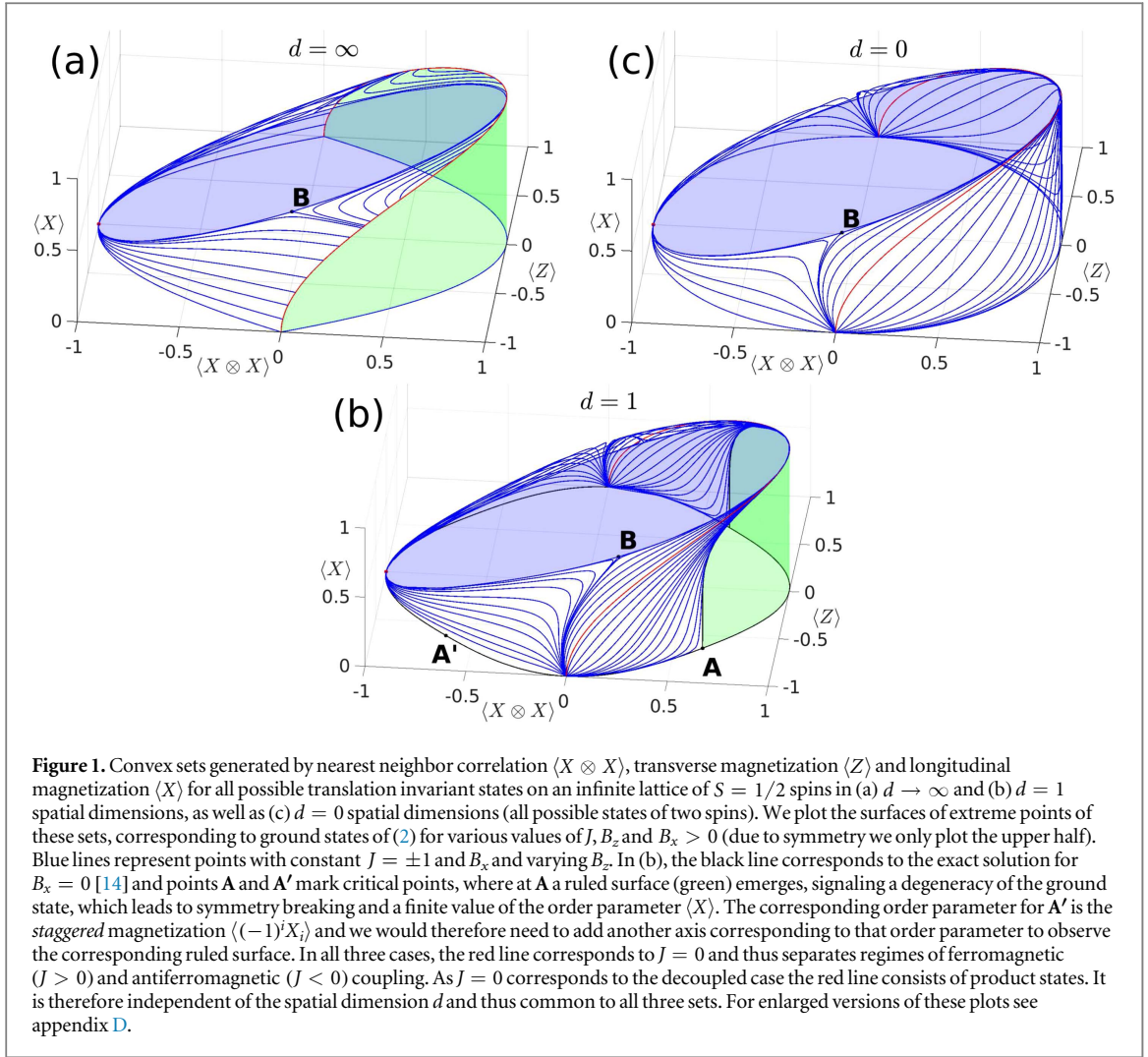
$$H = -\frac{2J}{K} \sum_{\langle ij \rangle} X_i X_j - B_z \sum_i Z_i - B_x \sum_i X_i. \quad (2)$$

In figure 1 we show the surface of this set in zero, one and infinite spatial dimensions (see appendix B.1 for a scatter plot and appendix D for enlarged versions of these surface plots).

For an infinite system in $d \geq 1$ spatial dimensions we witness the emergence of a ruled surface with all lines parallel to the new axis, which turns out to be the defining signature for symmetry breaking. Indeed, all points on such a line are ground states to the same instance of (2)—with parameters given by the orientation of the tangent plane⁴—but with different values of $\langle X \rangle$. This implies that the ground state is not unique and there is symmetry breaking, as an infinitesimal perturbation of the form of a longitudinal magnetic field $\epsilon \sum_i X_i$ to the Hamiltonian

³ When restricting oneself to RDMs of pure states, this problem is related to identifying the joint numerical range of a set of operators, which is not necessarily convex anymore [12, 13].

⁴ Here, all tangent planes with normal vectors $\vec{n} = (1, B_z, 0)$ with $|B_z| \leq 1$ will touch the set on a line of the ruled surface, instead of a single point.



(1) will break the symmetry, and make sure that the magnetization of the ground state will be polarized in the x -direction with a magnitude given by the extreme points of the convex set lying on the border of the ruled surface. $\langle X \rangle$ is then obviously the order parameter, and the shape of the border of the ruled surface encodes all the information about the ground state expectation values such as the order parameter as a function of the (transverse) magnetic field B_z .

Furthermore, from figure 1 we observe three additional remarkable but obvious facts. (i) The convex set of the zero-dimensional case completely contains the one-dimensional set, which in turn completely contains the infinite-dimensional case. This reflects the fact that more and more symmetry constraints (e.g. translation invariance along an increasing number of spatial dimensions) restrict the convex set of possible 2-site RDMs further and further. (ii) The ruled surfaces only arise in the thermodynamic limit, hence demonstrating the need for the well known fact that the order parameter is obtained by first taking the limit of the system size to infinity and only then the longitudinal magnetic field to zero. Any set obtained for a *finite* one-dimensional chain of N spins would look similar to (c). Put differently, with increasing N the surfaces of these sets will be gradually deformed to asymptotically yield the surface of set (b) as $N \rightarrow \infty$, i.e. only in this limit will the green ruled surface and thus symmetry breaking emerge. In [7, 8], the concept of speed was introduced to describe the curvature of convex sets of systems on finite lattices, and observed to diverge when doing finite size scaling. (iii) We can extract critical exponents by investigating the geometry of the convex set around the critical point⁵. More generally, any thermodynamic property of the system such as susceptibilities can be read off from this convex set and the properties of its surface, hence demonstrating the power of such convex set plots (for a detailed analysis in the case of classical lattice systems, see 3.4).

⁵ In the one-dimensional case, the dependence of $\langle X \rangle$ on the magnetic field B_z in the symmetry broken phase slightly below the critical point $B_z/J = 1 - \varepsilon$ with $\varepsilon \ll 1$ can be recovered from the orientation of the tangent plane $E = -J \langle X \otimes X \rangle - h \langle Z \rangle$ as $\frac{\partial \langle X \otimes X \rangle}{\partial \langle Z \rangle} = \varepsilon - 1$ to find that indeed in this regime $\langle X \rangle \propto \left(\frac{\partial \langle X \otimes X \rangle}{\partial \langle Z \rangle} + 1 \right)^{1/8}$.

Notice that the depicted convex sets with their ruled surfaces and non-analyticities exist prior to any reference to any underlying Hamiltonian. It is rather the choice of a collection of plotted observables (i.e. a choice of projection of the full convex set of RDMs) that enables access to thermodynamic properties of a corresponding Hamiltonian defined by this collection. The occurrence of symmetry breaking is therefore encoded in the geometrical structure of a certain projection of the convex set of all possible RDMs, and quantum phase transitions are a consequence of the geometry of such convex sets.

In the case where one would like to learn about symmetry breaking phase transitions of a particular Hamiltonian without knowing the order parameter, one can still use a random observable as additional axis. In general a random observable will have a finite contribution of the true order parameter, thus still generating ruled surfaces, albeit not with maximal extent. In order to find the true order parameter one can then optimize over random observables to obtain the maximal extent of the emerged ruled surfaces (see appendix C).

The general features of the plots in figure 1 are clearly generic for second order phase transitions. Note that in the case of first order phase transitions, one would *not* need to add an extra axis (corresponding to the order parameter) to witness symmetry breaking, and this would already be present at finite size (see section 3 and [9] for examples).

In figure 1 the surface of set (a) for $d \rightarrow \infty$ was numerically obtained using semidefinite programming: as a consequence of the monogamy properties of entanglement [10, 11] and the quantum de Finetti theorem [15], this set is equivalent to the convex set generated by all separable states [9, 16, 17]. For the particular case of two $S = 1/2$ spins, separability is completely determined by semidefinite constraints [18, 19] and the surface of the set can be obtained by minimizing the energy $E = -J \langle XX \rangle - B_z \langle Z \rangle - B_x \langle X \rangle$ with respect to all separable density matrices of two spins. Set (b) for $d = 1$ was obtained by doing extensive variational matrix product ground state calculations [20], while set (c) for $d = 0$ was obtained by exact diagonalization of a system of 2 spins.

2.1. Top plane

In all three sets of figure 1, point **B** marks the endpoint of a bifurcation line corresponding to $J = -1$, $B_x = 2$ and $B_z \rightarrow 0^+$, which leads up to a top (blue) plane.

The corresponding Hamiltonian at the top plane

$$H_{\text{TP}} = \frac{2}{K} \sum_{\langle ij \rangle} X_i X_j - 2 \sum_j X_j \quad (3)$$

is in fact classical and all eigenstates are product states in the x -basis $\{|+x\rangle, |-x\rangle\}$.

One can easily see that the ground state is exponentially degenerate with growing system size and for $d = 1$ the degeneracy is given by the Fibonacci sequence F_{N+1} where N is the number of lattice sites. The ground space is then given by all possible product states such that no two neighboring spins are in the $|-x\rangle$ state (see also section 3.2). Any linear combination of these states is a valid ground state and the entirety of all such possible states is given by the top blue plane.

To determine the edge of this plane for $d = 1$ we consider an infinitesimal perturbation

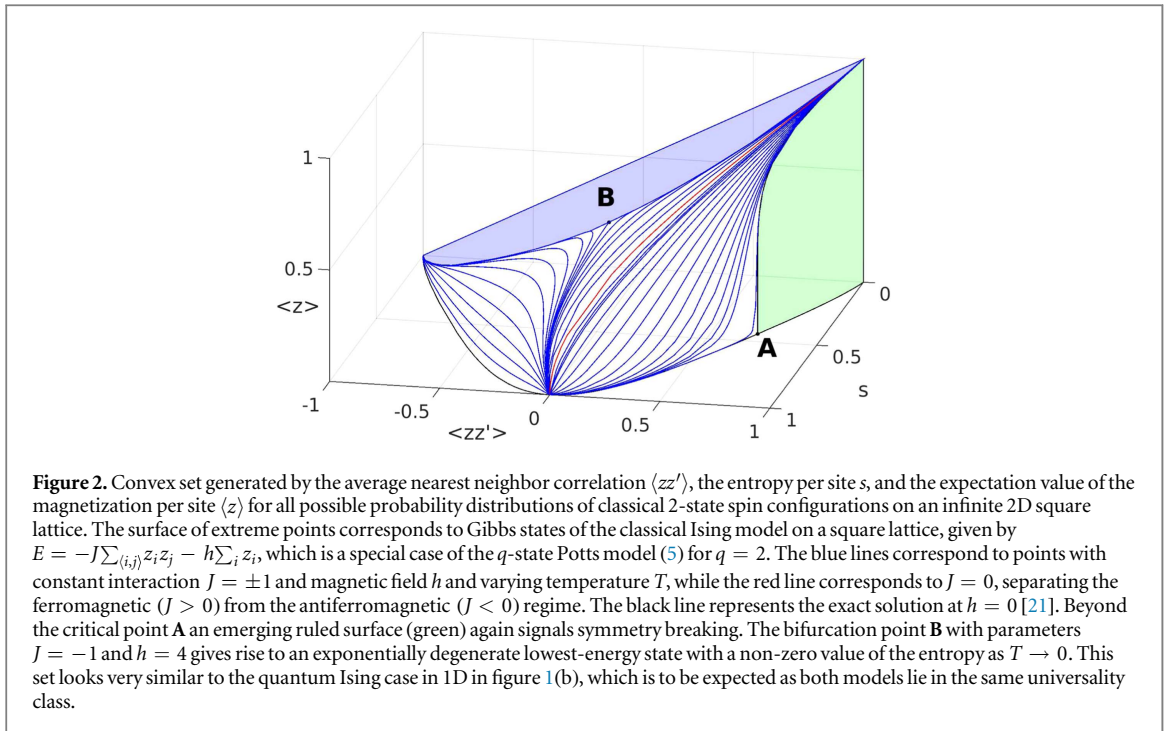
$H_1 = \alpha \sum_j X_j + \beta \sum_j Z_j$ away from this point, with $\alpha, \beta \ll 1$ and project this perturbation onto the Fibonacci subspace

$$H_p = \sum_i [1 + X_{i-1}][\alpha Z_i + \beta(X_i - 1)][1 + X_{i+1}]. \quad (4)$$

The points on the edge of the top blue plane then correspond to ground states of this projected Hamiltonian in the case of $d = 1$ spatial dimensions. In other words, for all values of α, β we seek linear combinations of states within the degenerate ground state subspace which maximize the magnetization along the direction $\mathbf{m} = [\alpha, 0, \beta]$. As the normal vector of the tangent plane is given by $\mathbf{n} = [J, B_z, B_x]$ this plane has the same orientation $\mathbf{n} = [-1, 0, 2]$ but slightly different boundaries in all three cases.

3. Convex sets for classical lattice systems

A natural question is whether a similar picture emerges in the case of classical statistical physics. As opposed to the competition between non-commuting terms in a quantum Hamiltonian, classical phase transitions emerge as a consequence of the competition between the internal energy E and the entropy S in the free energy $F = E - TS$. As the free energy is a linear function of energy and entropy, we expect similar convex sets as for the quantum case when making a scatter plot of the expectation values of energy, entropy and the order parameter with respect to all possible probability distributions (see figure 2 for the classical two-dimensional Ising model). Remarkably, we obtain a very similar picture as for the quantum case. The extreme points of the convex set now correspond to expectation values for Gibbs states which minimize the free energy. Note also that



pictures involving intensive quantities such as temperature and/or pressure on the axes would not make sense in this setting, as those quantities are not defined for general probability distributions out of equilibrium.

In the following we work out the case for a paradigmatic example of a classical lattice spin model in full detail: the q -state Potts model [22–25] is a generalization of the ubiquitous \mathbb{Z}_2 -symmetric Ising model [26, 27] to \mathbb{Z}_q -symmetry. It has been shown to correspond to a \mathbb{Z}_q lattice gauge theory of matter [28, 29] and in certain parameter regimes to coloring problems [30, 31] and hard-square lattice-gas models with nearest neighbor exclusion (1NN) [32].

The Potts model in a magnetic field is defined by the Hamiltonian

$$H(\mathbf{z}) = -J \sum_{\langle ij \rangle} \delta(z_i, z_j) - h \sum_j z_j, \quad (5)$$

where $z_i = 1, \dots, q$ is a q -state classical spin on site i , $\langle ij \rangle$ denotes nearest neighbors and δ is the Kronecker delta function. We consider the model in two spatial dimensions on a square lattice. At zero field, where the model possesses \mathbb{Z}_q -symmetry, it undergoes a symmetry breaking phase transition at finite critical inverse temperature $\beta_c = \log(\sqrt{q} + 1)$ [23, 33], above which the \mathbb{Z}_q -symmetry is spontaneously broken. For $q = 2$ the Potts model is equivalent to the classical Ising model [26] and can thus be solved exactly in zero field for all temperatures [21, 25]. For general $q > 2$ and zero field the model can be mapped onto a staggered six-vertex model, which can be solved exactly only at criticality [34, 35]. Other solvable cases include $J < 0$ at $T \rightarrow 0$ and zero field for $q = 3$ on the square lattice [30], and $q = 4$ on the hexagonal lattice as well as $q = 3$ on the Kagome lattice [31].

The symmetry breaking phase transition in zero field is continuous for $q \leq 4$ and of first order for $q > 4$ [23]. The nature of the phase transition will be apparent from the geometrical features of the corresponding convex set phase diagrams which we construct below.

Consider the space of all possible probability distributions $P(\mathbf{z})$ of configurations of q -state spins $z_i = 1, \dots, q$ with i the position on a two-dimensional square lattice with N sites, which form a convex set in some high-dimensional parameter space. In particular we consider three-dimensional projections of this set in the thermodynamic limit $N \rightarrow \infty$, parameterized by the three observables *nearest neighbor interaction energy per site*

$$\langle \delta(z, z') \rangle = \frac{1}{2N} \sum_{\langle ij \rangle} \langle \delta(z_i, z_j) \rangle, \quad (6)$$

shifted magnetization per site

$$\langle \tilde{z} \rangle = \langle z \rangle - \frac{q+1}{2} = \frac{1}{N} \sum_j \langle z_j \rangle - \frac{q+1}{2} \quad (7)$$

and entropy per site

$$s = -\frac{1}{N} \sum_{\mathbf{z}} P(\mathbf{z}) \log(P(\mathbf{z})), \quad (8)$$

where $\langle \dots \rangle$ denotes expectation values with respect to $P(\mathbf{z})$. The convex set \mathcal{C} is then given by all possible points $\mathbf{X} = [\langle \delta(z, z') \rangle, \langle \tilde{z} \rangle, s]$, such that $\langle \delta(z, z') \rangle$, $\langle \tilde{z} \rangle$ and s are compatible with each other, i.e. they stem from a common valid probability distribution $P(\mathbf{z})$. This is an instance of the classical marginal problem [36–39]. Notice that we are using a shifted magnetization with an offset $\frac{q+1}{2}$, such that the convex set is reflection symmetric with respect to $\langle \tilde{z} \rangle$. The extreme points on the surface of this set are then naturally given by Gibbs states of (5).

To see this, consider (hyper)planes in this three-dimensional parameter space, which are defined as families of points $\mathbf{X} \in \mathcal{C}$, related by a plane equation of the form

$$\mathbf{n} \cdot \mathbf{X} = n_x \langle \delta(z, z') \rangle + n_y \langle \tilde{z} \rangle + n_z s = \|\mathbf{n}\| d, \quad (9)$$

where \mathbf{n} is the normal vector of the plane and d is the distance of the hyperplane to the origin. Setting $n_x = 2J$, $n_y = h$ and $n_z = T$, this yields exactly the (negative of the) free energy per site of (5)

$$-f = 2J \langle \delta(z, z') \rangle + h \langle \tilde{z} \rangle + Ts, \quad (10)$$

where the factor 2 comes from the fact that every site has 4 nearest neighbors on a two-dimensional square lattice.

For a given set of parameters (i.e. normal vector) the hyperplane *tangent* to the convex set has maximum possible distance from the origin and thus also minimizes the free energy, which is the definition of a Gibbs state. Every point on the surface thus corresponds to a state of thermodynamic equilibrium, at parameters given by the orientation of the tangent plane and free energy proportional to the distance of the tangent plane to the origin. Conversely, every point inside the convex set corresponds to a possible non-equilibrium state of the system.

If the tangent plane touches the convex set at a unique point only, then the thermodynamic stable state is unique and exactly given by a Gibbs state which yields the observables given by the tangent point for the parameters (J, h, T) defined by the orientation of the tangent plane, i.e. its normal vector \mathbf{n} . If however the tangent plane touches the set on an entire line or even a plane, then the state which minimizes the free energy for these parameters is not unique, which is a prerequisite of symmetry breaking. The set of valid states can then be parameterized by one (or more) real parameters. Such ruled surfaces (continuous sets of tangent lines) or planes are thus the geometrical signatures that will enable us to detect symmetry breaking and the emergence of a connected order parameter.

We show the surfaces of the resulting convex sets for the Potts model for $q = 3$ and $q = 5$ in figures 3 and 4 respectively (the special case of the Ising model, corresponding to $q = 2$, is shown in figure 2). These sets show interesting geometrical features from which a wealth of other information, such as the nature of phase transitions, locations of critical points, critical exponents, susceptibilities, etc can be extracted. The numerical data for plotting these surfaces has been obtained by means of tensor network techniques described in appendix A. For scatter plots of points obtained from random probability distributions, which approximate the convex set from the inside, see appendix B.2.

3.1. Symmetry breaking and the ruled surface

For zero field, $J > 0$ and $T < T_c$ the thermodynamic state that minimizes the free energy is q -fold degenerate and the \mathbb{Z}_q -symmetry can be spontaneously broken, such that $\langle \tilde{z} \rangle \neq 0$. The maximum possible value $\langle \tilde{z} \rangle_{\max}$ can then be taken as the order parameter associated to this phase transition⁶. For a given set of parameters any state within this q -fold degenerate space thus minimizes the free energy and is characterized by the same values for $\langle \delta(z, z') \rangle$ and s , but different $\langle \tilde{z} \rangle$ ⁷.

This is nicely reflected in the convex sets through the emergence of a (green) ruled surface at the critical point. Zero field implies tangent planes with normal vectors lying in the $\langle \tilde{z} \rangle = 0$ plane, i.e. $\mathbf{n} = [2J, 0, T]$. The tangent plane touches the convex set on a unique point in the $\langle \tilde{z} \rangle = 0$ plane everywhere except for $J > 0$ and $T < T_c$, where the tangent plane in fact touches the convex set along a whole line for each J and T , given by $\mathbf{X}(t) = [\langle \delta(z, z') \rangle, r \langle \tilde{z} \rangle_{\max}, s]$ with $r \in [-1, 1]$ and $\langle \tilde{z} \rangle_{\max} > 0$ the maximum value of the order parameter.

⁶ Given $\langle \tilde{z} \rangle_{\max}$ the shifted magnetization is then $\langle \tilde{z} \rangle = (k - (q + 1)/2) \langle \tilde{z} \rangle_{\max}$ with $k = 1, \dots, q$ the integer enumerating the maximally symmetry broken states, characterized by one-site marginal distributions given by $p(z) = 1/q + p(2\delta_{z,k} - 1)$, where $p < 1/q$ is a function of T . Other order parameters for the Potts model have also been proposed. One possibility for defining an observable whose expectation value in the symmetry broken phase is independent of k is e.g. given by defining $O(z) = \exp(2\pi iz/q)$ and measuring $|\langle O \rangle| = pq \in [0, 1]$.

⁷ Mixtures of maximally symmetry broken states generally do not correspond to physically realizable states as they cannot be converted into each other by means of local modifications. Mathematically they are elements of disjoint Hilbert space sectors [40, 41]. A hint towards this fact is given by the peculiar structure of the random scatter plots for quantum and classical systems as shown in appendix B.

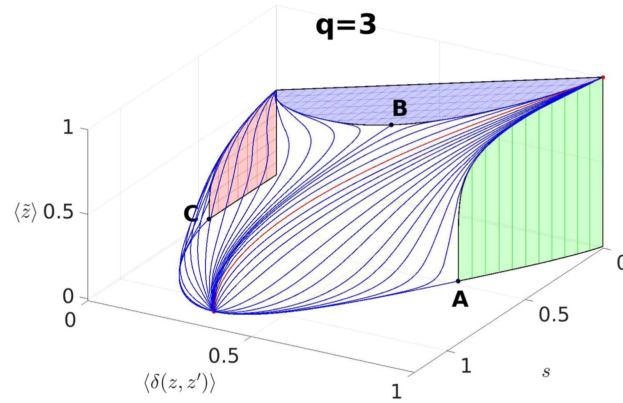


Figure 3. Convex set generated by nearest-neighbor interaction energy $\langle \delta(z, z') \rangle$, shifted magnetization $\langle \bar{z} \rangle$ and entropy per site s of all possible probability distributions of 3-state spins on a two-dimensional square lattice. We plot the surface of this set, corresponding to Gibbs-states of (5) for $q = 3$. Due to reflection symmetry we only plot the upper half of the set. Blue lines denote points of constant $J = \pm 1$ and h and varying temperature T . The red line denotes the exactly solvable decoupled case $J = 0$ and thus separates regions of ferromagnetic and antiferromagnetic coupling. At the critical point **A** the emergence of a (green) ruled surface signals a non-uniqueness of the thermal equilibrium state at zero field and thus symmetry breaking. As a guide to the eye we have plotted a few vertical lines on the ruled surface, along which the tangent plane touches the convex set. Point **B** marks the end point of the bifurcation line of $J = -1, h = 4$ and $T \rightarrow 0$, leading up to the (blue) top plane where the lowest energy state is exponentially degenerate, resulting in a finite residual entropy as described in section 3.2. A similar situation arises at point **C**, corresponding to the end point of the line $J = -1, h = 0, T \rightarrow 0$. There again the lowest energy state is exponentially degenerate, resulting in a finite residual entropy as described in section 3.3. This plane is only present for $q > 2$ and does therefore not appear in the convex set drawn for the Ising model in figure 2. As a guide to the eye we have drawn two-dimensional grids onto the top and left plane, emphasizing the fact that there the tangent plane touches the set on the entire respective planes.

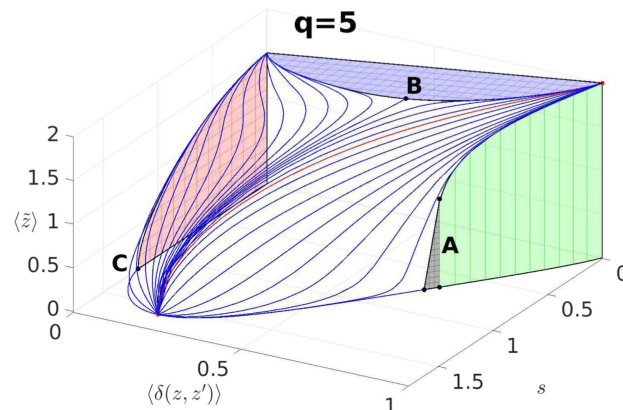


Figure 4. Convex set generated by the same observables as in figure 3 for the case of 5-state spins where the surface of this set is given by Gibbs-states of (5) for $q = 5$. For $q > 4$ the phase transition is of first order and thus comes with a discontinuity of the three observables at the critical point. This results in a coexistence region of the ordered and disordered phases and the critical point **A** gets stretched out into a (gray) flat triangular surface, where any mixture of the two phases is a valid state, i.e. the two phases coexist. This flat part then smoothly connects to the (symmetry broken) ordered phase represented by the green ruled surface. As a guide to the eye we have drawn a two-dimensional grid onto the flat triangular surface, emphasizing the fact that there the tangent plane touches the set on the entire triangular surface and we have also plotted a few vertical lines on the green ruled surface, along which the tangent plane touches the convex set. The flat surfaces emerging from points **B** and **C** are of the same nature as described in figure 3.

An infinitesimal value of $h \neq 0$ then immediately explicitly breaks the symmetry and causes the tangent plane to touch the set on a *unique* point of the set infinitesimally close to the edge of the ruled surface. Or equivalently, the curve of tangent points of a tangent plane given by $\mathbf{n} = [2J, h \neq 0, T]$ as $h \rightarrow 0^\pm$ will end in a point with $\langle \bar{z} \rangle = \pm \langle \bar{z} \rangle_{\max} \neq 0$ for $T < T_c$. This nicely reflects the fact that the order parameter can be obtained by first taking the thermodynamic limit at non-zero field before letting the field go to zero.

The nature of the phase transition changes from continuous to first order for $q > 4$, where a first order phase transition is characterized by a latent heat and a discontinuity of first derivatives of the free energy at the critical point. The internal energy and all other expectation values that can be written as a derivative of the free energy, such as the order parameter and also the entropy per site s therefore have a discontinuity at the critical point. In the convex set we can thus detect first order phase transitions through the appearance of *flat hyperplanes* at the boundary that arise *even without additionally plotting the order parameter*. At the critical point

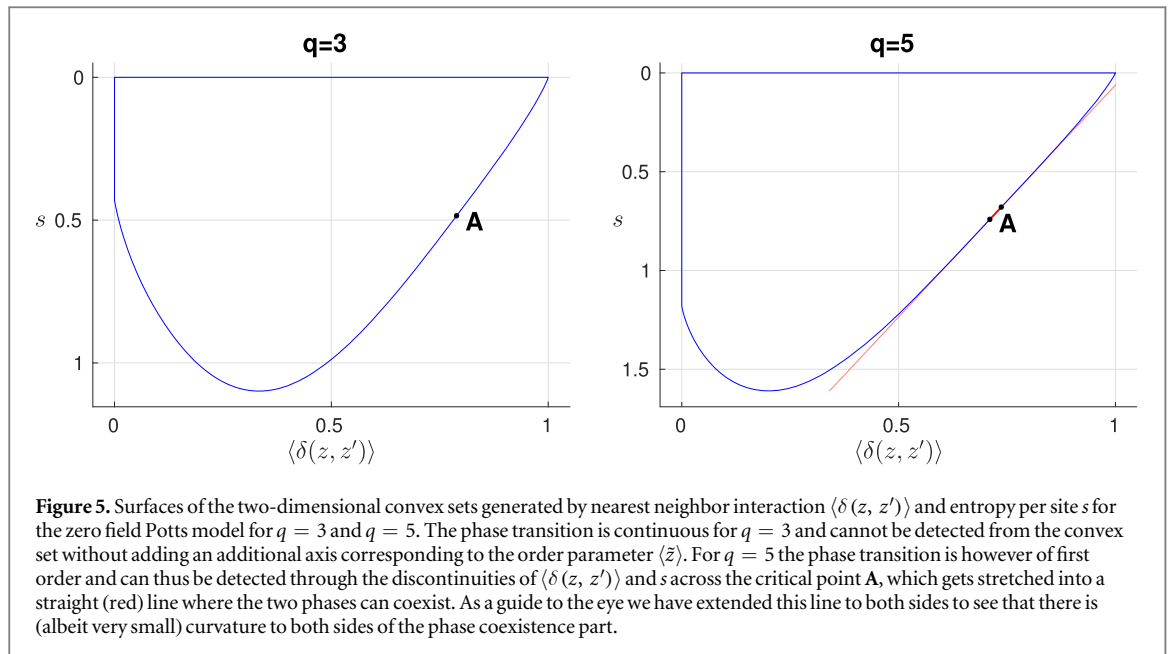


Figure 5. Surfaces of the two-dimensional convex sets generated by nearest neighbor interaction $\langle \delta(z, z') \rangle$ and entropy per site s for the zero field Potts model for $q = 3$ and $q = 5$. The phase transition is continuous for $q = 3$ and cannot be detected from the convex set without adding an additional axis corresponding to the order parameter $\langle \bar{z} \rangle$. For $q = 5$ the phase transition is however of first order and can thus be detected through the discontinuities of $\langle \delta(z, z') \rangle$ and s across the critical point A, which gets stretched into a straight (red) line where the two phases can coexist. As a guide to the eye we have extended this line to both sides to see that there is (albeit very small) curvature to both sides of the phase coexistence part.

the thermal equilibrium state is not unique and any point on this hyperplane is a valid state of the system *at the critical temperature*. This corresponds to the coexistence of phases at the critical point which is characteristic for first order phase transitions. In the case of the Potts model, this flat hyperplane then smoothly connects to the ruled surface representing the symmetry broken phase $T < T_c$ (see figure 4).

For continuous phase transitions the thermodynamic state at the critical point is still unique and there is no such additional hyperplane. We can thus already detect first order phase transitions in the lower dimensional convex set that does not include the order parameter. In the case of the Potts model, a two-dimensional convex set parameterized by $\langle \delta(z, z') \rangle$ and s thus already suffices to detect the phase transition for $q > 4$, it will however show no signature of the phase transition for $q \leq 4$ (see figure 5), for which adding an additional axis corresponding to the order parameter $\langle \bar{z} \rangle$ is necessary.

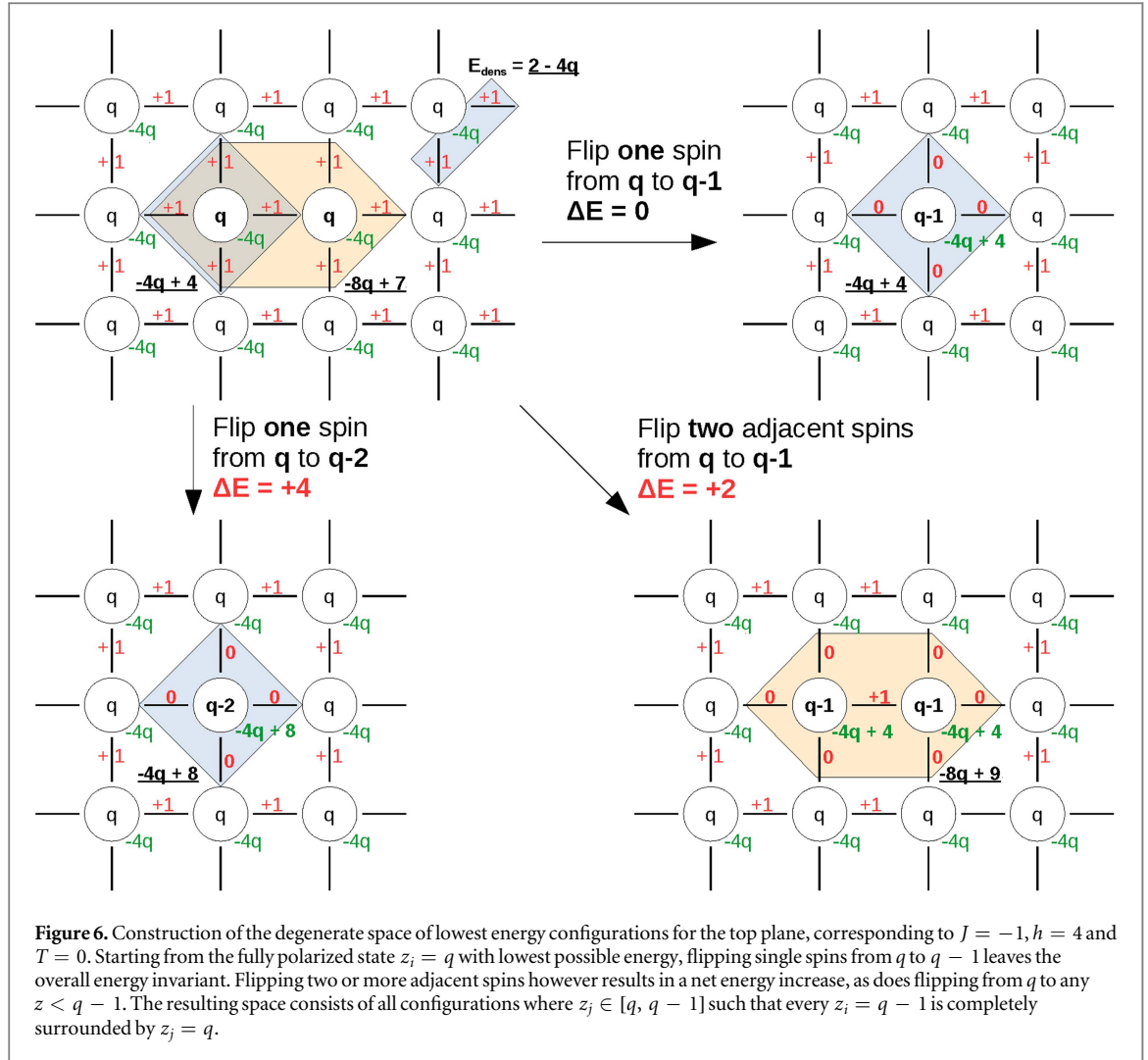
We want to emphasize here that these convex sets and thus also the ruled surfaces exist prior to making any references to any model Hamiltonian, we just consider finite dimensional projections of the convex set of all possible probability distributions of a system of physical degrees of freedom. This means that the reason for the occurrence of symmetry breaking phase transitions ultimately lies in the geometrical structure of the space of all possible probability distributions. It would therefore be interesting to investigate all possible projections of this set and classify all possible ruled surfaces that can arise on such projections.

3.2. Top plane

The top (blue) plane corresponds to parameters $J = -1, h = 4$ and $T = 0$ where the tangent plane touches the convex set on the entire top plane, meaning that the thermal equilibrium state is not unique and in fact all states on this plane are valid equilibrium states for these parameters.

Exactly at this point, the two terms in the Hamiltonian become ‘equally strong’ in the following sense. If we start from the completely polarized state $z_j = q$, the magnetic field term is minimized, whereas the interaction part has a positive energy contribution, resulting in a net energy of $2-4q$ per site. If we now flip one spin at an arbitrary position from q to $q - 1$, we gain exactly the same amount of energy from the interaction term as we lose from the magnetic field term and the overall energy stays the same. We can now continue flipping spins that way without changing the energy, as long as we never flip any spins *next to an already flipped one*, which would result in a net energy increase of $+2$. In general, a cluster of N_f flipped spins and a boundary of length N_b results in a net energy change of $4N_f - N_b \geq 0$, which is only zero for $N_f = 1$. The two lowest energy states with the smallest magnetization are thus the two Néel states between q and $q - 1$. Similarly, flipping from q to any $z < q - 1$ always results in a net energy increase and the restricted space of lowest energy states is thus given by all configurations $z_j \in [q, q - 1]$ such that every $z_i = q - 1$ is completely surrounded by $z_j = q$ (see also figure 6). This restricted space is equivalent to the configuration space for the nearest-neighbor exclusion lattice-gas model (1NN) [32] and grows exponentially with the system size.

At $T = 0$ all such configurations are equally likely; the entropy per site is therefore finite and measures the exponential growth of the space of lowest energy configurations. This symmetry of equal probability can however be spontaneously broken as any statistical mixture of such configurations is a valid state of the system



with equal free energy $f = 2 - 4q$. The entirety of all such mixtures is exactly given by the top blue plane in the convex sets, where point **B** marks the state of equal probability which has maximal entropy.

To calculate the boundary of the top blue plane we consider tiny perturbations away from this point in parameter space, which immediately cause a jump onto the edge of the plane. Similar to degenerate perturbation theory we then simulate this perturbation Hamiltonian only within the restricted subspace of the top plane to lift the exponential degeneracy and determine its extreme points. The perturbation Hamiltonian is just the magnetic field term

$$\beta H_1 = \mu \sum_j z_j, \quad (11)$$

where μ is usually small. Since we however simulate this Hamiltonian in the *restricted* subspace only (which also makes the simulation non-trivial), μ need not be small and just controls the position along the edge of the top plane. We therefore wish to evaluate

$$Z = \sum_{z \in \mathcal{Z}_t} e^{-\mu \sum_j z_j}, \quad (12)$$

where the sum is only over the space of valid configurations \mathcal{Z}_t given by the top plane and $\mu \in \mathbb{R}$. The entropy per site s is then given by

$$s = \log(z) + \mu \langle z \rangle, \quad (13)$$

where $z = Z^{1/N}$ is the partition function per site. The other observables $\langle \delta(z, z') \rangle$ and $\langle \bar{z} \rangle$ are computed as usual but with respect to (12). Note that entropy and $\langle \delta(z, z') \rangle$ are independent of q and $\langle \bar{z} \rangle$ for different q are related by just an offset. The top plane thus has the *same shape* for all q , but different vertical offset in $\langle \bar{z} \rangle$.

Note that (12) is equivalent to the 1NN model in a chemical potential μ [42–44], where states q and $q - 1$ correspond to an empty and occupied site respectively. The limits $\mu \rightarrow \pm\infty$ correspond to the the completely polarized and the Néel states respectively (or equivalently the completely empty and maximally filled lattice

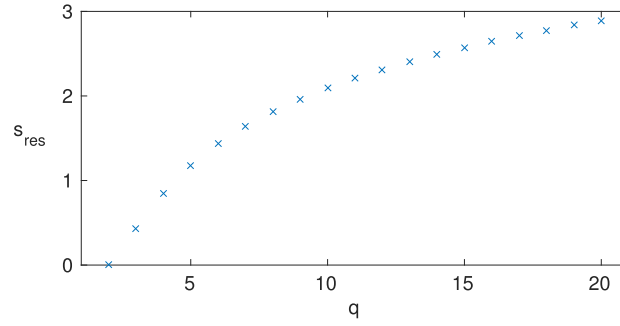


Figure 7. Residual entropy at point C on the left plane, corresponding to $J = -1, h = 0$ and $T = 0$, for values $q \in [2, 20]$. Here the residual entropy corresponds to the logarithm of the number of configurations (per site) such that no two neighbors are in the same state.

respectively in terms of the 1NN model) and thus have zero entropy, while $\mu = 0$ corresponds to point B with maximal residual entropy s_{res} . Our calculated value at this point reproduces the (log of the) value $\kappa(1)$ given in section 1.1 of [32] up to machine precision. The tensor network we use to simulate (12) is described in appendix A.1.

3.3. Left plane

The left (red) plane with $\langle \delta(z, z') \rangle = 0$ corresponds to parameters $J = -1, h = 0$ and $T = 0$ where the tangent plane touches the convex set on the entire left plane, meaning that the thermal equilibrium state is not unique and in fact all states on this plane are valid equilibrium states for these parameters.

For these parameters the lowest energy states are given by all configurations $z_j \in [1, q]$, such that *no nearest neighbors are in the same state*. This is the famous vertex coloring problem and consequently, the partition function can be written as a chromatic polynomial in q [45, 46] and counts the number of proper vertex colorings of the two-dimensional square lattice with q colors. For any $q > 2$ the number of valid configurations is exponentially large in system size and we are thus presented with the same situation as for the top plane in the previous section, but with a different restricted subspace. For $q = 2$ this problem is trivial as only two valid configurations exist (the two Néel states) and the left plane is absent (see figure 2).

Again, at $T = 0$ all these configurations are equally likely, leading to a residual, non-zero entropy s_{res} . For $q = 3$ this can be mapped onto the problem of residual entropy of square ice [30], for which the value is known exactly as $s_{\text{res}} = 3/2 \log(4/3)$ [47, 48]. For $q > 3$ there are no exact solutions for the square lattice. The symmetry of equal probability can again be spontaneously broken and any point on the left flat surface then corresponds to a valid statistical mixture of configurations within the restricted subspace, giving the same free energy $f = 0$. All these mixtures are represented by the left red plane in the convex sets, where point C corresponds to the equal probability mixture which has maximal entropy s_{res} .

To determine the boundary of the left red plane we proceed the same way as in section 3.2 and simulate

$$Z = \sum_{z \in \mathcal{Z}_c} e^{-\mu \sum_j z_j}, \quad (14)$$

where the sum is now over all proper vertex colorings \mathcal{Z}_c . The entropy is again given by (13).

We have calculated s_{res} for several values of q (see figure 7), where we can reproduce the exact value for $q = 3$ up to an accuracy of $\mathcal{O}(10^{-10})$ with bond dimension $D = 800$ of the MPS-representation of the dominant eigenvector of the transfer matrix.

The tensor network used to simulate (14) is described in appendix A.2.

3.4. Critical exponents and susceptibilities

If we are given the entire convex set as a function of the extensive observables we can determine critical exponents and susceptibilities purely from the geometrical shape of its surface, i.e. completely independent from the intensive parameters J, T and h . To ease notation in this section we will write

$$t := \langle \delta(z, z') \rangle, \quad z := \langle \tilde{z} \rangle. \quad (15)$$

Critical exponents for $q \leq 4$ can be extracted from the change of the tangent plane orientation around the critical point. For this we need the functional relation between an observable and a model parameter close to the critical point. As an example consider the shifted magnetization z for zero field slightly below the critical temperature T_c . There we expect z to behave as

$$z \propto \left(1 - \frac{T}{T_c}\right)^b, \quad h = 0 \quad (16)$$

with b the critical exponent for the magnetization.

We assume the thermodynamic surface to be given e.g. by the interaction energy t as a function of the (independent) variables entropy s and shifted magnetization z , i.e. $t = t(s, z)$. Our intention is to extract b entirely from the geometrical form of the thermodynamic surface, i.e. from the surface given by the function $t(s, z)$. We therefore need a way to express the model parameters J , T and h in terms of the observables t , s and z . From (9) and (10) we saw that they are precisely the elements of the normal vector to the surface function $t(s, z)$. On the other hand, the normal vector to the thermodynamic surface $t(s, z)$ at a given point is

$$\mathbf{n} = \left[1, -\frac{\partial t}{\partial s}, -\frac{\partial t}{\partial z}\right]. \quad (17)$$

and we can immediately identify

$$T = -2J \frac{\partial t}{\partial s}, \quad h = -2J \frac{\partial t}{\partial z}. \quad (18)$$

Without loss of generality we fix $J = 1$ and consider the case $h = 0$, i.e. the path of normal vectors with $n_3 = -\frac{\partial t}{\partial z} = 0$. We can then write

$$\log z = b \log \left[1 - \frac{\partial t}{\partial s} \left(\frac{\partial t}{\partial s} \Big|_A\right)^{-1}\right] + \text{const}, \quad (19)$$

where we have extracted the critical temperature from the orientation of the tangent plane at the critical point \mathbf{A} as $T_c = -2 \frac{\partial t}{\partial s} \Big|_A$. If we plot $\log \left[1 - \frac{\partial t}{\partial s} \left(\frac{\partial t}{\partial s} \Big|_A\right)^{-1}\right]$ versus $\log z$ we expect a linear relation near \mathbf{A} and we can read off b from the slope⁸.

Estimates for the critical exponents calculated that way from the obtained given numerical data are of the same accuracy as estimates obtained from conventional fits of observables versus model parameters (i.e. a logarithmic fit of (16)).

Furthermore, susceptibilities defined as the derivatives of the (extensive) observables t , s and z with respect to the (intensive) model parameters J , T and h can be calculated from the curvature of the surface. Loosely speaking, we would like to know how we move on the surface if we change the orientation of the normal vector infinitesimally along one component. In other words, if we change the orientation of \mathbf{n} by δT along n_2 , what are the resulting δt , δs and δz . The relation between these changes is of course dictated by the function $t(s, z)$ (or in fact any other representation of the surface, e.g. as $s(t, z)$ or $z(t, s)$).

With fixed $J = 1$ we have established the model parameters as functions purely of the observables in (18), i.e. we consider the vector-valued function

$$\mathbf{p}(s, z) = [T(s, z), h(s, z)]. \quad (20)$$

According to (17) the Jacobian of this function is then proportional to the Hessian of $t(s, z)$ via

$$J_p = \begin{bmatrix} \frac{\partial T}{\partial s} & \frac{\partial T}{\partial z} \\ \frac{\partial h}{\partial s} & \frac{\partial h}{\partial z} \end{bmatrix} = -2 \begin{bmatrix} \frac{\partial^2 t}{\partial s^2} & \frac{\partial^2 t}{\partial s \partial z} \\ \frac{\partial^2 t}{\partial s \partial z} & \frac{\partial^2 t}{\partial z^2} \end{bmatrix}, \quad (21)$$

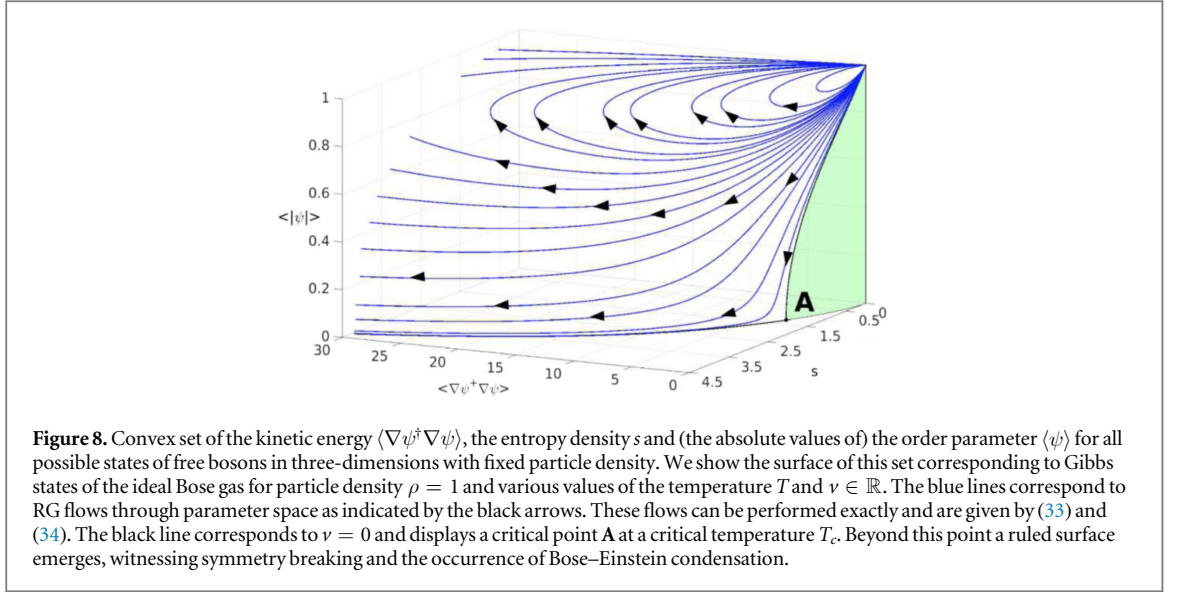
so we can express it purely in terms of the observables. The infinitesimal change in the normal vector when moving infinitesimally on the surface is then given by $\delta \mathbf{p} = J_p \cdot \delta \mathbf{O}$ with $\delta \mathbf{O} = [\delta s, \delta z]$.

We are however interested in the converse direction, i.e. the derivatives which are the elements of the Jacobian of the inverse function $\mathbf{O}(T, h) := \mathbf{p}^{-1}(T, h) = [s(T, h), z(T, h)]$

$$J_o = \begin{bmatrix} \frac{\partial s}{\partial T} & \frac{\partial s}{\partial h} \\ \frac{\partial z}{\partial T} & \frac{\partial z}{\partial h} \end{bmatrix}. \quad (22)$$

The inverse function theorem then gives the elements of this Jacobian by inverting (21) and we can thus obtain the susceptibilities from the second derivatives of $t(s, z)$, i.e. we can obtain $\delta \mathbf{O} = J_o \cdot \delta \mathbf{p} = J_p^{-1} \cdot \delta \mathbf{p}$. With the

⁸ As per definition of the ruled surface, z is not unique along this path and it is understood that we take the maximum of z in (19) for each s and t , i.e. the order parameter. This path is nothing but the upper boundary of the ruled surface shown e.g. in figure 3. Alternatively we could have formulated (19) in terms of derivatives of $s = s(t, z)$. Notice however that $z = z(s, t)$ is not a good choice as it is a highly multivalued function on the ruled surface.



determinant of (21) given by

$$\det J_p = 4 \left[\frac{\partial^2 t}{\partial s^2} \frac{\partial^2 t}{\partial z^2} - \left(\frac{\partial^2 t}{\partial s \partial z} \right)^2 \right] \quad (23)$$

we get e.g.

$$\chi_T = \frac{\partial z}{\partial T} = \frac{1}{2} \left[\frac{\partial^2 t}{\partial s^2} \frac{\partial^2 t}{\partial z^2} - \left(\frac{\partial^2 t}{\partial s \partial z} \right)^2 \right]^{-1} \frac{\partial^2 t}{\partial s \partial z} \quad (24)$$

$$= \frac{1}{2} \left[\frac{\partial^2 t}{\partial s^2} \frac{\partial^2 t}{\partial z^2} \left(\frac{\partial^2 t}{\partial s \partial z} \right)^{-1} - \frac{\partial^2 t}{\partial s \partial z} \right]^{-1}, \quad (25)$$

$$\chi_h = \frac{\partial z}{\partial h} = -\frac{1}{2} \left[\frac{\partial^2 t}{\partial s^2} \frac{\partial^2 t}{\partial z^2} - \left(\frac{\partial^2 t}{\partial s \partial z} \right)^2 \right]^{-1} \frac{\partial^2 t}{\partial s^2} \quad (26)$$

$$= \frac{1}{2} \left[\left(\frac{\partial^2 t}{\partial s \partial z} \right)^2 \left(\frac{\partial^2 t}{\partial s^2} \right)^{-1} - \frac{\partial^2 t}{\partial z^2} \right]^{-1}. \quad (27)$$

These relations are only valid if (21) is invertible and the susceptibilities can diverge if (23) becomes zero.

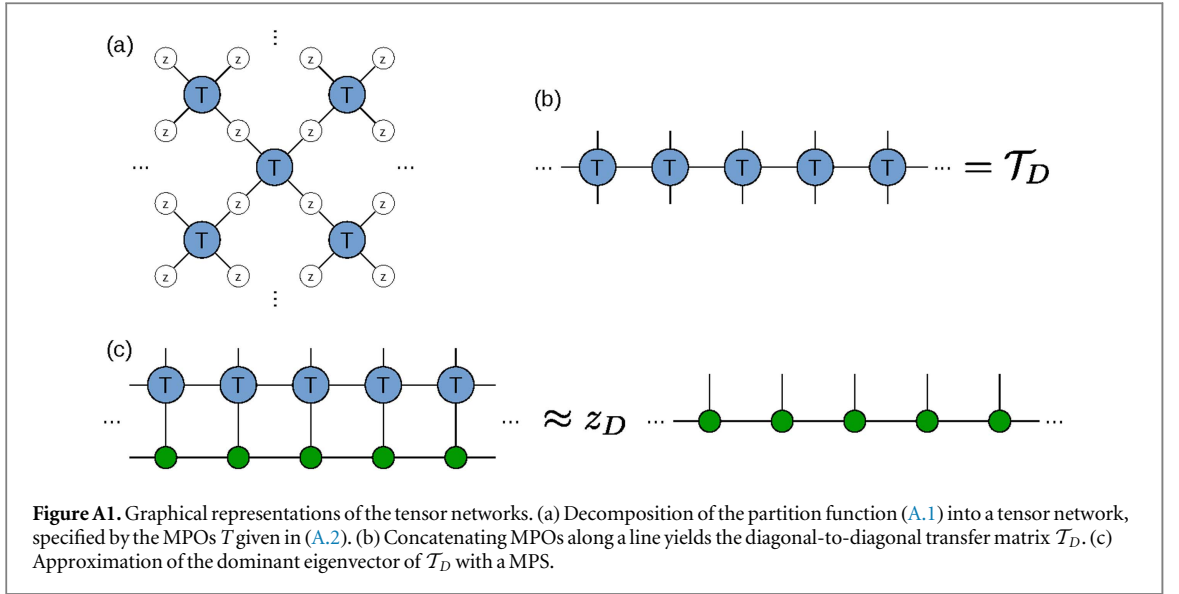
Consider for example the magnetic susceptibility χ_T . In figure 3 along the path $h = 0$ we have $z = 0$ and $\frac{\partial t}{\partial z} = 0$ (i.e. normal vectors with $n_3 = 0$), as t becomes maximal when $z = 0$. This is the case for any s along this path, the mixed derivative $\frac{\partial^2 t}{\partial s \partial z}$ is thus also zero everywhere. For $T > T_c$ the second derivative $\frac{\partial^2 t}{\partial z^2}$ is finite, but becomes zero as $T \rightarrow T_c^+$ (and is in fact zero at every point on the ruled surface per definition). With $\frac{\partial^2 t}{\partial s \partial z} = 0$ and $\frac{\partial^2 t}{\partial z^2} \rightarrow 0$ the determinant of the Jacobian becomes zero as $T \rightarrow T_c$ and χ_T diverges.

4. Convex sets for quantum field theories

As a final example, let us consider a 3D quantum system of free bosons in the continuum at finite temperature where we expect to witness Bose–Einstein condensation. Motivated by the above findings we plot the expectation value of the kinetic energy, the entropy, and a $U(1)$ symmetry breaking order parameter $\langle \psi \rangle$, with respect to all possible quantum states to obtain a meaningful convex structure (see figure 8). The extreme points of this set correspond to Gibbs states of the Hamiltonian

$$H = \int_V d^3x \frac{1}{2m} \nabla \psi^\dagger(x) \nabla \psi(x) - \nu [\psi(x) + \psi^\dagger(x)] \quad (28)$$

at fixed density $\rho = 1$, where again a symmetry breaking term has been added explicitly. A ruled surface emerging below the critical temperature for $\nu = 0$ beautifully signals the onset of Bose–Einstein condensation, where the equilibrium state is not unique and can be parameterized by a finite value of $\langle \psi \rangle$. Again, the critical exponent can be extracted from the change of the orientation of the tangent plane around the critical point.



The system of an ideal Bose gas in the presence of a $U(1)$ -symmetry breaking term can be solved analytically [49] and the thermodynamic extensive quantities plotted in figure 8 are readily found to be

$$\langle \psi \rangle = -\frac{\nu}{\mu}, \quad (29)$$

$$s = \frac{5}{2} \lambda^3 F_{5/2}(-\beta\mu) - \beta\mu \lambda^3 F_{3/2}(-\beta\mu), \quad (30)$$

$$E_{\text{kin}} = \frac{3}{2} \beta^{-1} \lambda^3 F_{5/2}(-\beta\mu) \quad (31)$$

with s the entropy density and the chemical potential μ always chosen such that

$$\rho = \frac{\nu^2}{\mu^2} + \lambda^3 F_{3/2}(-\beta\mu) = 1. \quad (32)$$

Further we have defined $\lambda^2 = \frac{2\pi}{mT}$ and $F_\sigma(x) = \sum_{n=1}^{\infty} n^{-\sigma} e^{-nx} \quad \forall x \geq 0$. At $\nu = 0$ the critical temperature is given by $T_c(\rho) = \frac{2\pi}{m\lambda_c^2}$ with $\lambda_c^3 = \rho^{-1} F_{3/2}(0)$.

The blue lines in figure 8 correspond to momentum-shell RG-flows through parameter space, which can be performed exactly [50]. The RG flow equations are found to be

$$\beta(s) = \beta(0) e^{-2s}, \quad (33)$$

$$\nu(s) = \nu(0) e^{\frac{7}{2}s} \quad (34)$$

for $s \in (-\infty, \infty)$.

5. Conclusion

In conclusion, we investigated the convex structure of RDMs and marginal probability distributions of many body systems and illustrated how the concept of symmetry breaking emerges very naturally through the appearance of ruled surfaces at the boundaries of these sets. As these sets exist without any prior notion of an underlying Hamiltonian, this shows that the reason for the occurrence of symmetry breaking lies in the geometrical structures of the convex sets of all possible RDMs or marginal probability distributions. This picture seems to capture all the thermodynamically relevant features of many body systems in an extremely concise way. It would therefore be very interesting to classify all possible ruled surfaces that can arise on such convex sets.

Our work is very close in spirit to the original groundbreaking papers of Gibbs [2, 51], which clarified that phase transitions and the coexistence of different phases can be understood in terms of non-analyticities in the parametrization of the surface of thermodynamic diagrams. It is also related to ideas developed in the context of N -representability [5–8] for describing quantum phase transitions in fermionic systems. It provides an explicit construction of the famous thermodynamic surface of Maxwell [3] for the case of classical and quantum spin systems, and illustrates very concisely the mathematical physics point of view of symmetry breaking as a breakdown of ergodicity [41]. It also complements the ideas developed in [52, 53], where a systematic procedure for finding order parameters was developed by contrasting the RDMs of the low-lying excited states in finite size

quantum many body systems. Note however that the starting point of our work is very different: we make no *a priori* reference to a Hamiltonian, and just consider scatter plots with respect to all possible many body wavefunctions and/or probability distributions. Only the choice of plotted observables relates the obtained convex set to the ground/equilibrium state properties of a corresponding Hamiltonian. Finally, the works [16, 17] reported on the convex structure of expectation values of separable density matrices; in retrospect, those are the convex sets obtained in the mean-field regime of an infinite-dimensional lattice, as illustrated in figure 1(a).

One remaining open question is how phase transitions of different types, such as e.g. Berezinskii–Kosterlitz–Thouless phase transitions [54, 55] or especially phase transitions in the ground states of two- and higher-dimensional quantum systems with topological order fit in this description, as these cannot be characterized in terms of local order parameters. The tensor network description of quantum states might yield one possible resolution, as the topological order induces certain symmetries onto the virtual boundary theory of the tensor network [56–58]. Topological phase transitions then correspond to symmetry-breaking phase transitions in the virtual boundary theory [59], i.e. in the structure of the fixed-point subspace of the transfer matrix of the tensor network. These transitions can thus be characterized in terms of a local order parameter at the virtual level of the tensor network [60]. By bringing this virtual operator back to the physical level, it can be associated to the non-local string order parameters that characterize the topological phase [61]. When considering systems on a torus, the natural approach would hence be to plot the expectation value of such a Wilson loop around the torus; the different ground states in the topological phase can then be distinguished by different values of this (non-extensive and non-local) order parameter, and hence a ruled surface should emerge at the topological phase transition. Convex sets for SPT phases have been constructed in [62], which appeared as a follow up to the preprint [63] of the current paper.

Acknowledgments

We thank J I Cirac, C Dellago, W De Roeck, M Mariën and D Nagaj for inspiring discussions. This work was supported by the Austrian Science Fund (FWF): F4104 SFB ViCoM and F4014 SFB FoQuS, ERA Chemistry and the EC through grants QUTE and SIQS.

Appendix A. Tensor network representations for classical spin lattice models

In this section we give information about the tensor network representations of the thermal partition function Z and the tensor network methods used to approximately calculate the partition function z per site, the entropy per site s and the expectation values of local observables (such as $\langle \delta(z, z') \rangle$ and $\langle z \rangle$) of Gibbs states of (5).

Consider a two-dimensional square lattice with $N = 2L^2$ sites where the partition function is given by

$$Z = \sum_{\mathbf{z}} \exp[-\beta H(\mathbf{z})] = \sum_{\mathbf{z}} \prod_{\langle ij \rangle} \exp\{\beta [J\delta(z_i, z_j) + \frac{h}{4}(z_i + z_j)]\}, \quad (\text{A.1})$$

and can be understood as a contraction of a tensor network consisting of 4-index tensors

$$T_{z_i, z_j, z_k, z_l} = \exp\{\beta J [\delta(z_i, z_j) + \delta(z_i, z_k) + \delta(z_j, z_l) + \delta(z_k, z_l)]\} \\ \times \exp\left[\frac{\beta h}{2}(z_i + z_j + z_k + z_l)\right]. \quad (\text{A.2})$$

Such that

$$Z = \text{tTr} \left(\prod_{n=1}^{N/2} T \right) = \sum_{\mathbf{z}} T_{z_i, z_j, z_k, z_l} T_{z_l, z_m, z_n, z_o} T_{z_o, z_p, z_q, z_r, z_s} T_{z_s, z_t, z_u, z_v} \dots, \quad (\text{A.3})$$

where tTr denotes the tensor trace. Notice that every index appears exactly twice. Since every tensor (A.2) contains 4 nearest neighbor interaction terms and Z comprises exactly $2N$ of such terms there are half as many tensors in the network as there are sites on the lattice.

A concatenation of this choice of tensor along a line throughout the entire lattice yields the diagonal-to-diagonal transfer matrix (DTM) \mathcal{T}_D of the partition function, or in other words, T represents a matrix product operator (MPO) [64, 65] decomposition of the DTM. Other tensor decompositions—e.g. yielding the row-to-row or column-to-column transfer matrix upon concatenation—are also possible, the advantage of (A.2) is however that the DTM is hermitian for all J, h and β .

We therefore have $Z = \text{Tr}(\mathcal{T}_D^L)$ and in the limit $N \rightarrow \infty$ the dominant eigenvalue of the DTM corresponds to the partition function per diagonal $z_D = Z^L$ of the system (see e.g. [25]).

In order to evaluate the partition function per site $z = Z^{\frac{1}{N}} = z_B^{\frac{1}{N}}$ and the local observables in the thermodynamic limit $L \rightarrow \infty$ we obtain the dominant eigenvector of the DTM by means of matrix product state (MPS) [65] techniques. More specifically, we use a modification of the algorithm presented in [20] for MPOs in the thermodynamic limit [66] to calculate the partition function per site z and an MPS approximation of the dominant eigenvector of the DTM, which can be used to calculate all local observables, in particular $\langle \delta(z, z') \rangle$ and $\langle \tilde{z} \rangle = \langle z \rangle - \frac{q+1}{2}$.

As we have access to the partition function per site z , we can now easily evaluate the entropy per site, which is given by

$$s = \beta e - \beta f = \beta e + \log(z), \quad (\text{A.4})$$

with the internal energy per site $e = -2J \langle \delta(z, z') \rangle - h \langle z \rangle$. For graphical representations of the tensor network and related quantities see figure A1.

A.1. Top plane and the 1NN

In order to determine the boundary of the top plane we simulate the trivial perturbation Hamiltonian in the restricted subspace \mathcal{Z}_t given by all configurations $z_j \in [q, q-1]$ such that every $z_i = q-1$ is completely surrounded by $z_j = q$, i.e. we wish to evaluate

$$Z_{\text{tp}} = \sum_{z \in \mathcal{Z}_t} e^{-\mu \sum_j z_j}. \quad (\text{A.5})$$

In section 3.2 it is also mentioned that (A.5) is equivalent to the 1NN model in a chemical potential [32, 42–44] by interpreting $z_j = q, q-1$ as empty and occupied sites of a lattice gas with nearest neighbor exclusion. We can therefore arrive at a formulation of (A.5) where the entropy per site s and the interaction $\langle \delta(z, z') \rangle$ are independent of q and $\langle \tilde{z} \rangle$ for different q are related by an offset.

By substituting $z_j = q - s_j$ with $s_j = 0, 1$ we get

$$Z_{\text{tp}} = \sum_{s \in \mathcal{S}} e^{-\mu \sum_j (q - s_j)} = e^{-\mu q N} \sum_{s \in \mathcal{S}} e^{\mu \sum_j s_j} = e^{-\mu q N} Z_{\text{hs}}, \quad (\text{A.6})$$

where Z_{hs} is the partition function of the 1NN model and \mathcal{S} is the restricted set of all configurations $s_j \in [0, 1]$ such that every $s_i = 1$ is completely surrounded by $s_j = 0$. The partition functions per site are then related by $z_{\text{tp}} = e^{-\mu q} z_{\text{hs}}$.

To evaluate Z_{hs} we can achieve a summation over the restricted subspace only by summing over all configurations $s_j \in [0, 1]$, but giving configurations with neighboring $s_i = s_j = 1$ statistical weight zero. This way we obtain a MPO decomposition with bond dimension 2, with MPOs given by

$$T_{s_i s_j s_k s_l}^{\text{hs}} = f_{s_i s_j} f_{s_i s_k} f_{s_j s_l} f_{s_k s_l} \exp \left[\frac{\mu}{2} (s_i + s_j + s_k + s_l) \right], \quad (\text{A.7})$$

where the 2×2 matrix f is given by

$$f_{s_i s_j} = 1 - s_i s_j. \quad (\text{A.8})$$

The magnetization then becomes

$$\langle z \rangle = -\frac{\partial \log z_{\text{tp}}}{\partial \mu} = q - \frac{\partial \log z_{\text{hs}}}{\partial \mu} = q - \langle s \rangle. \quad (\text{A.9})$$

Giving for the entropy per site

$$s = \log z_{\text{tp}} + \mu \langle z \rangle = \log z_{\text{hs}} - \mu \langle s \rangle. \quad (\text{A.10})$$

$\langle \delta(z, z') \rangle$ is invariant as $\delta(z_i, z_j) = \delta(s_i, s_j)$ and the expectation value is evaluated with respect to the same probability distribution.

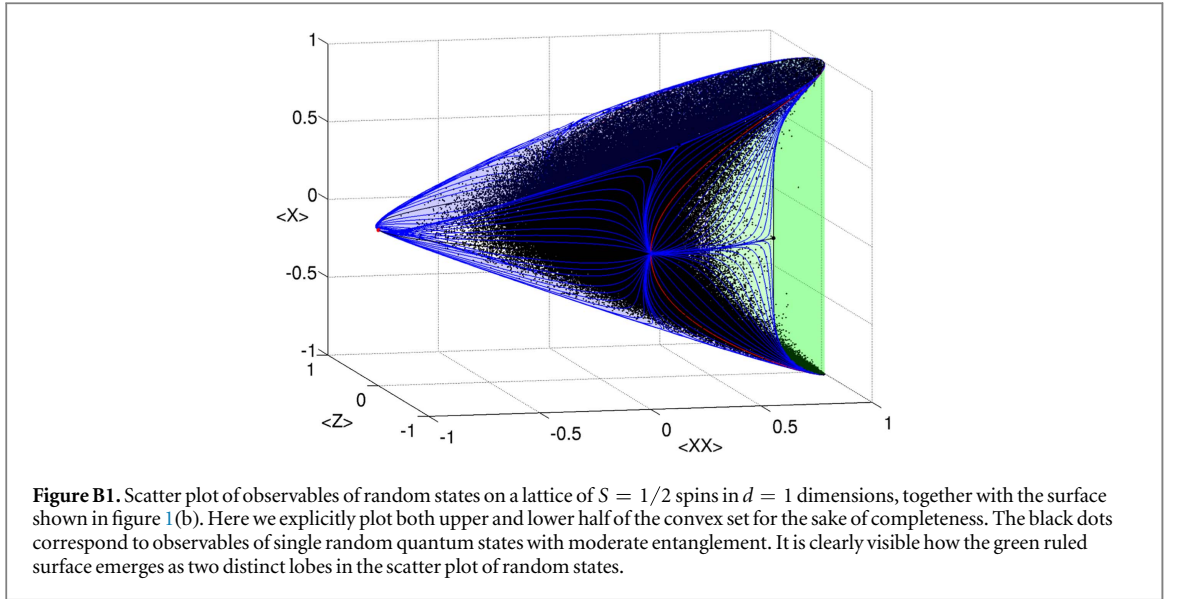
A.2. Left plane and the coloring problem

To determine the boundaries of the left (red) plane we seek to simulate the same perturbation Hamiltonian as in the last section

$$Z_{\text{lp}} = \sum_{z \in \mathcal{Z}_c} e^{-\mu \sum_j z_j}, \quad (\text{A.11})$$

but with \mathcal{Z}_c a different restricted subspace, given by all configurations $z_j \in [1, q]$ such that no nearest neighbors have the same value.

We can again achieve a summation over the restricted subspace only by summing over all configurations $z_j \in [1, q]$, but giving configurations with neighboring $z_i = z_j$ statistical weight zero. This way we obtain a MPO decomposition with (unchanged) bond dimension q , with MPOs given by



$$T_{z_i, z_j, z_k, z_l}^{\text{lp}} = f_{z_i, z_j} f_{z_i, z_k} f_{z_j, z_l} f_{z_k, z_l} \exp \left[-\frac{\mu}{2} (z_i + z_j + z_k + z_l) \right], \quad (\text{A.12})$$

where the $q \times q$ matrix f is given by

$$f_{z_i, z_j} = 1 - \delta(z_i, z_j). \quad (\text{A.13})$$

The expectation value of the interaction $\langle \delta(z, z') \rangle$ is zero per construction and the entropy is then given by

$$s = \log z_{\text{lp}} + \mu \langle z \rangle. \quad (\text{A.14})$$

Appendix B. Random scatter plots

B.1. One-dimensional quantum spin-1/2 lattice systems

In figure B1 we show a scatter plot of observables of random states on a lattice of $S = 1/2$ spins in $d = 1$ dimensions, together with the surface already shown in figure 1(b). The points in the plot were obtained by generating a large amount of random infinite matrix product states [65] of low matrix dimension $D = 2 - 10$, drawn from the unitary ensemble [67] and measuring the corresponding observables. The plot gives a beautiful practical demonstration of the procedure outlined in section 2. There it is argued that a scatter plot generated from drawing random states and calculating expectation values of local observables from (in this case) the 2-site RDM produces a convex set, whose surface is given by points corresponding to ground states of a family of Hamiltonians defined by the chosen collection of observables (in this case (2)). For a given set of Hamiltonian parameters, any points inside the set correspond to 2-site RDMs from (superpositions or mixtures of) excited states with respect to that Hamiltonian.

The surface shown in figure 1(b) is asymptotically obtained by taking the convex hull of the data points generated from a larger and larger amount of random states with varying bond dimension. Figure B1 however shows that moderate bond dimensions of $D = 2 - 10$ already yield a very good approximation of the true surface. The scatter plot also beautifully shows how the ruled surface emerges from the cloud of random data points in the form of two distinct lobes in the vicinity of the green ruled surface with hardly any points in between, whereas away from the the ruled surface the data points are distributed fairly homogeneously. We observe this to be the characteristic geometric phenomenon for the occurrence of symmetry breaking in terms of a random scatter plot and suspect that it can be related to the breakdown of ergodicity and the existence of disjoint Hilbert space sectors in phases of spontaneously broken symmetries [40, 41].

B.2. Two-dimensional classical lattice spin systems

In section 3 we have built on the fact that the surface of the convex sets are given by Gibbs states of (5), which can be efficiently simulated using tensor network techniques. As these convex sets however exist in probability space prior to any definition of a Hamiltonian, the occurrence of symmetry breaking is thus purely a consequence of the geometrical structure of probability space. To further elucidate this argument we show scatter plots of points from random probability distributions $P(z)$, which are not Gibbs distributions. The points generated by

expectation values with respect to these distributions must therefore all lie within the convex set surfaces shown in figures 3 and 4.

In order to simulate random probability distributions we resort to the class of distributions representable by tensor networks consisting of 4-index tensors T

$$P(\mathbf{z}) = \prod T = T_{z_0, z_1, z_2, z_3} T_{z_1, z_2, z_3, z_4} T_{z_2, z_3, z_4, z_5} T_{z_3, z_4, z_5, z_6} \dots, \quad (\text{B.1})$$

such that the partition function, obtained by summing over all configurations \mathbf{z} , is given by a tensor trace

$$Z = \text{tTr}(\prod T) = \sum_{\mathbf{z}} T_{z_0, z_1, z_2, z_3} T_{z_1, z_2, z_3, z_4} T_{z_2, z_3, z_4, z_5} T_{z_3, z_4, z_5, z_6} \dots, \quad (\text{B.2})$$

which can again be efficiently evaluated using tensor network techniques. The expectation values $\langle \delta(z, z') \rangle$ and $\langle \bar{z} \rangle$ can then be calculated the usual way (see appendix A).

For a general (unnormalized) probability distribution $P(\mathbf{z})$ the entropy per site is given by

$$s(P) = - \sum_{\mathbf{z}} P(\mathbf{z}) \log[P(\mathbf{z})] = \log(z) - \frac{1}{N} \langle \log(P) \rangle, \quad (\text{B.3})$$

with z the partition function per site. In the special case of a Gibbs distribution, $\langle \log(P) \rangle$ is nothing but the internal energy times the inverse temperature βE , which is a local observable (i.e. a sum of local terms). The entropy is then given by the familiar formula $s = \beta(e - f)$, with e the internal energy per site and f the free energy per site.

For arbitrary $P(\mathbf{z})$ the quantity $\frac{1}{N} \langle \log P \rangle$ is in general however not a local observable. With (B.1) on the other hand we essentially restrict ourselves to probability distributions, for which the entropy is given by the sum of local observables and the entropy per site can be evaluated as

$$s = \log(z) - \frac{1}{2} \langle \log T \rangle. \quad (\text{B.4})$$

The factor $\frac{1}{2}$ comes from the fact that there are half as many tensors T as there are sites on the lattice. We thus obtain random points within the convex set by sampling T (or rather $\log T$) from some probability distribution and measuring $\langle \delta(z, z') \rangle$, $\langle \bar{z} \rangle$ and s according to (B.4).

The class of distributions given by (B.1) contains all possible nearest-neighbor interactions as well as 4-site interactions around the face on every other plaquette. Higher order interactions and distances can be achieved in principle by blocking sites, i.e. transforming to variables $z'_i = \otimes_{r=1}^R z_r$. The bond dimension of T is then given by q^R and only moderate values of R are computationally feasible. As a demonstration we have however resorted to $R = 1$ and have drawn $\log(T)$ from a gaussian distribution with varying standard deviation $\sigma \in [0.2, 1.5]$. The resulting scatter plots for $q = 3$ and $q = 5$ are shown in figure B2, together with the surfaces of extreme points already plotted in figures 3 and 4.

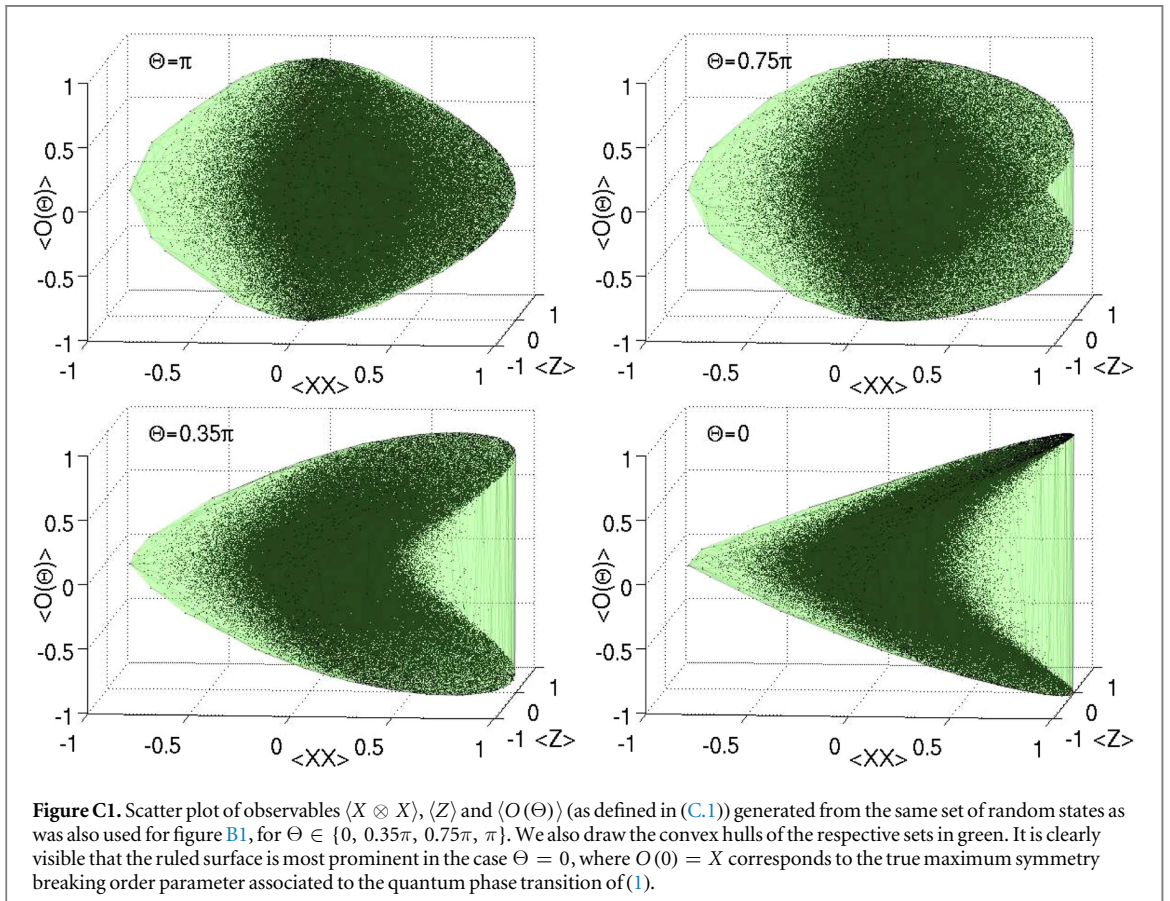
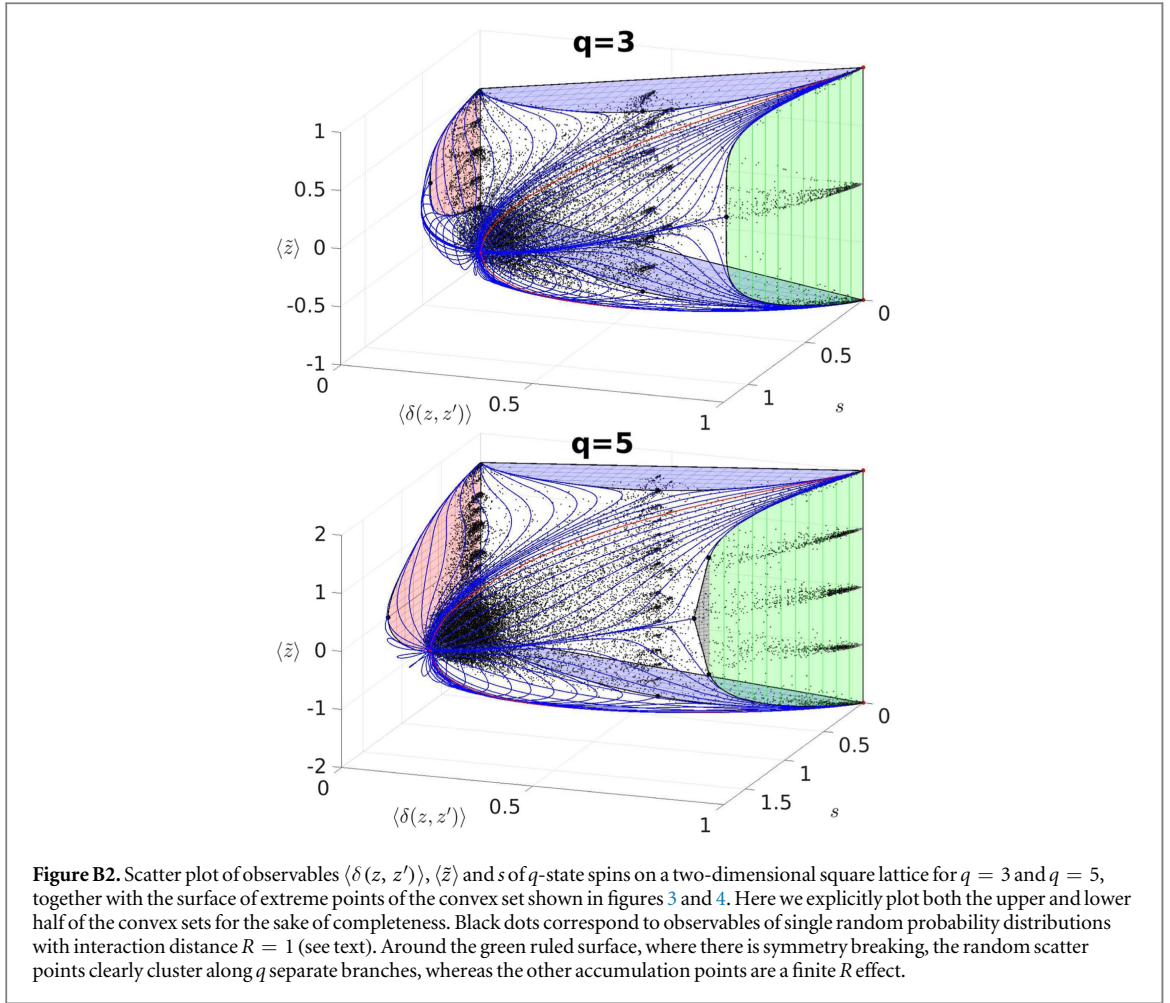
These surfaces are asymptotically obtained by taking the convex hull of more and more random points generated that way with $R \rightarrow \infty$. Figure B2 shows that $R = 1$ already gives a quite good qualitative approximation of the convex set. Especially around the green ruled surface where we expect spontaneous symmetry breaking it is apparent that the points cluster along q distinct branches. This can be interpreted as a signature of the existence of q disjoint probability spaces in the symmetry broken phase and thus statistical mixtures of configurations from different sectors do not correspond to physically realizable states.

Appendix C. Order parameter optimization

It is argued in section 2 that in the case where the order parameter with maximal symmetry breaking is not known, one can still use a random observable, which will in general have a finite overlap with the true order parameter. Using this observable as an additional axis will thus yield a convex body showing a ruled surface, albeit not with maximal extent. One can then optimize over all possible observables of that type to find the observable which maximizes the extent of the ruled surface and thus corresponds to the order parameter with maximal symmetry breaking.

We demonstrate this procedure in the case of the quantum Ising model (1). We assume the order parameter to be a local one-site observable and thus optimize over all possible linear combinations of Pauli-matrices X , Y and Z , with fixed spectral radius. If the order parameter is not a one-site observable one would have to optimize over multi-site observables, i.e. over linear combinations of products of Pauli-matrices in the case of spin-1/2 systems. Along that line it would be very interesting to know if it is possible to *a priori* determine (possibly by different means) just from a random scatter plot if there is a symmetry breaking order parameter at all.

As the observable Z however is already present in the Hamiltonian itself (i.e. we already plot $\langle Z \rangle$), it is enough to consider only linear combinations of X and Y . We thus define the one-parameter family of observables



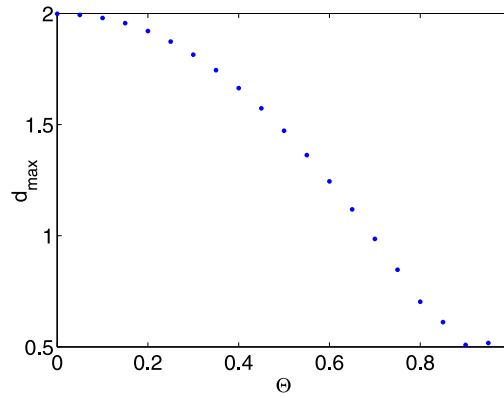


Figure C2. Maximum distance d_{\max} of neighboring points on the convex hull as defined in (C.2), versus angle Θ . This quantity clearly takes its maximum value of $d_{\max} = 2$ at $\Theta = 0$, where $O(0) = X$.

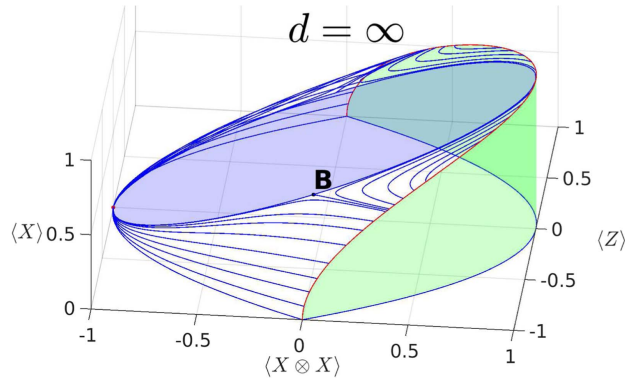


Figure D1. Enlarged version of the plot shown in figure 1(a).

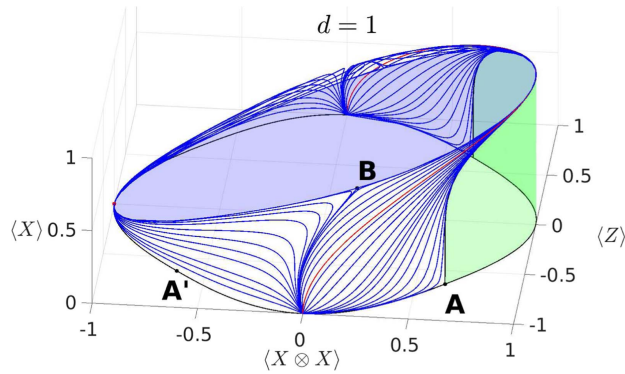
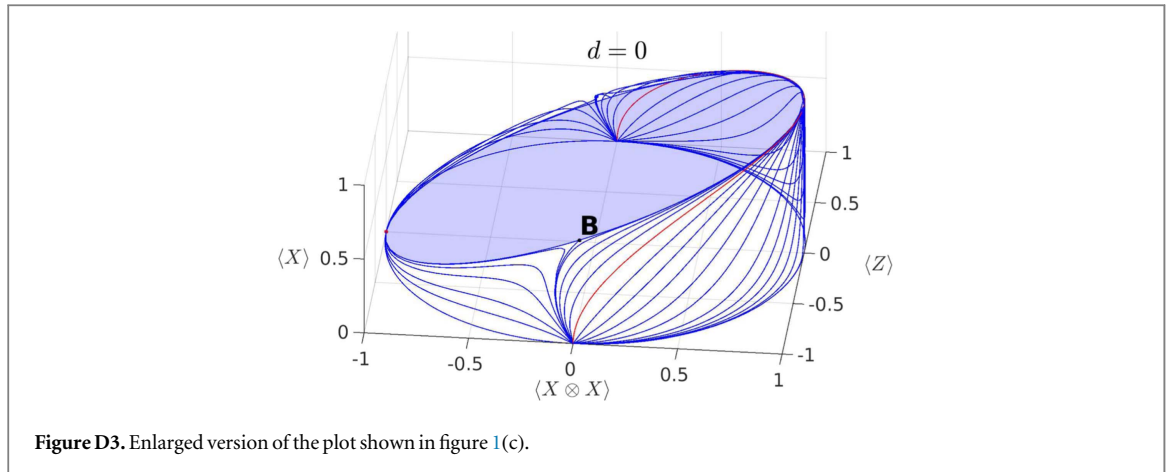


Figure D2. Enlarged version of the plot shown in figure 1(b).

$$O(\Theta) = \cos(\Theta/2)X + \sin(\Theta/2)Y, \quad 0 \leq \Theta < \pi. \tag{C.1}$$

And construct convex sets from random states, using $\langle O(\Theta) \rangle$ as a third axis, and vary Θ . Figure C1 shows instances of these sets, together with their convex hulls, for certain selected values of Θ , all generated from the same collection of random states that was also used to generate figure B1. It is clearly visible that the ruled surface in the form of a distinct lobe structure is most prominent for $O(\Theta = 0) = X$, whereas there is absolutely no signature of a ruled surface for $O(\Theta = \pi) = Y$.



To quantify the extent of the ruled surface emerging in these plots we calculate the maximum distance

$$d_{\max} = \max_{(ij)} |x_i - x_j|, \quad (\text{C.2})$$

where x_i and x_j are neighboring points on the convex hull of the set. This quantity is naturally maximized when the optimal order parameter with maximum symmetry breaking is used as a third axis and is plotted against Θ for the present case in figure C2, where d_{\max} shows a definite maximum at $\Theta = 0$.

As visual characterization in terms of ruled surfaces becomes especially hard for convex sets in more than three-dimensions (i.e. with more than three observables), (C.2) can serve as a good quantity to detect ruled surfaces also in these cases.

Appendix D. Enlarged plots for quantum lattices

In figures D1–D3 we show enlarged version of the convex sets shown in figure 1 for better visibility of the sets' details.

References

- [1] Gibbs JW 1873 *Trans. Conn. Acad.* II **382–404** 309–42 (<https://archive.org/details/scientificpaper00gibbgoog>)
- [2] Gibbs JW 1876 *Trans. Conn. Acad.* III **343–524** 108–248 (<https://archive.org/details/scientificpaper00gibbgoog>)
- [3] Maxwell JC 1871 *Theory of Heat* (New York: Dover)
- [4] van der Waals JD 1891 *Arch. Néerlandaises* **24** 1
- [5] Coulson CA 1960 *Rev. Mod. Phys.* **32** 170
- [6] Erdahl RM and Jin B 2000 *On Calculating Approximate and Exact Density Matrices Many-Electron Densities and Density Matrices* (Dordrecht: Kluwer) p 57
- [7] Gidofalvi G and Mazziotti DA 2006 *Phys. Rev. A* **74** 012501
- [8] Schwerdtfeger CA and Mazziotti DA 2009 *J. Chem. Phys.* **130** 224102
- [9] Verstraete F and Cirac JI 2006 *Phys. Rev. B* **73** 094423
- [10] Bennett CH, DiVincenzo DP, Smolin JA and Wootters WK 1996 *Phys. Rev. A* **54** 3824
- [11] Terhal BM 2004 *IBM J. Res. Dev.* **48** 71
- [12] Dash AT 1972 *Glas. Mat.* **73** 75
- [13] Gutkin E and Życzkowski K 2013 *Linear Algebr. Appl.* **438** 2394
- [14] Pfeuty P 1970 *Ann. Phys.* **57** 79
- [15] Werner RF 1989 *Lett. Math. Phys.* **17** 359
- [16] Verstraete F, Dehaene J and de Moor B 2002 *J. Mod. Opt.* **49** 1277
- [17] Bengtsson I and Życzkowski K 2008 *Geometry of Quantum States: An Introduction to Quantum Entanglement* (Cambridge: Cambridge University Press)
- [18] Peres A 1996 *Phys. Rev. Lett.* **77** 1413
- [19] Horodecki M, Horodecki P and Horodecki R 1996 *Phys. Lett. A* **223** 1
- [20] Haegeman J, Cirac JI, Osborne TJ, Pizorni I, Verschelde H and Verstraete F 2011 *Phys. Rev. Lett.* **107** 070601
- [21] Onsager L 1944 *Phys. Rev.* **65** 117
- [22] Ashkin J and Teller E 1943 *Phys. Rev.* **64** 178
- [23] Potts RB 1952 *Proc. Camb. Phil. Soc.* **48** 106–9
- [24] Wu FY 1982 *Rev. Mod. Phys.* **54** 235–68
- [25] Baxter RJ 1982 *Exactly Solved Models in Statistical Mechanics* (New York: Dover)
- [26] Ising E 1925 *Z. Phys.* **31** 253
- [27] Brush S 1967 *Rev. Mod. Phys.* **39** 883
- [28] Balian R, Drouffe JM and Itzykson C 1975 *Phys. Rev. D* **11** 2098
- [29] Kogut JB 1979 *Rev. Mod. Phys.* **51** 659

- [30] Baxter R J 1970 *J. Math. Phys.* **11** 3116
- [31] Baxter R J 1970 *J. Math. Phys.* **11** 784
- [32] Baxter R J 1999 *Ann. Comb.* **3** 191
- [33] Hinterman A, Kunz H and Wu F Y 1978 *J. Stat. Phys.* **19** 623
- [34] Temperley H N V and Lieb E H 1971 *Proc. R. Soc. A* **322** 251
- [35] Baxter R J 1973 *J. Phys. C: Solid State Phys.* **65** L445
- [36] Klyachko A 2002 Coherent states, entanglement, and geometric invariant theory arXiv:quant-ph/0206012
- [37] Dall'Agglio G, Kotz S and Salinetti G (ed) 1991 *Advances in Probability Distributions with Given Margins* (Dordrecht: Kluwer)
- [38] Rüschemdorf L, Schweizer B and Taylor M (ed) 1996 *Distributions with Fixed Marginals and Related Topics* (Hayward: Institute of Mathematical Statistics)
- [39] Benes V and Stépán J (ed) 1997 *Distributions with Given Margins and Moment Problem* (Dordrecht: Kluwer)
- [40] Strocchi F 2005 *Symmetry Breaking* (New York: Springer)
- [41] Fannes M, Pule J V and Verbeure A 1983 *Helv. Phys. Acta* **55** 391
- [42] Gaunt D S and Fisher M E 1965 *J. Chem. Phys.* **43** 2840
- [43] Guo W and Blöte H W J 2002 *Phys. Rev. E* **66** 046140
- [44] Fernandes H, Arenzon J and Levin Y 2007 *J. Chem. Phys.* **126** 114508
- [45] Fortuin C M and Kasteleyn P W 1972 *Physica* **57** 536
- [46] Tutte W T 1967 *J. Comb. Theory* **2** 301
- [47] Lieb E H 1967 *Phys. Rev. Lett.* **18** 692
- [48] Lieb E H 1967 *Phys. Rev.* **162** 162
- [49] Gunton J D and Buckingham M J 1968 *Phys. Rev.* **166** 152
- [50] Singh K K 1981 *Pramana J. Phys.* **16** 211
- [51] Israel R B 1979 *Convexity in the Theory of Lattice Gases* (Princeton, NJ: Princeton University Press)
- [52] Furukawa S, Misguich G and Oshikawa M 2006 *Phys. Rev. Lett.* **96** 047211
- [53] Henley C L and Changlani H J 2014 *J. Stat. Mech.* **P11002**
- [54] Berezinskii V L 1970 *Zh. Eksp. Teor. Fiz.* **59** 907–20
Berezinskii V L 1971 *Zh. Eksp. Teor. Fiz.* **61** 1144–56
- [55] Kosterlitz J M and Thouless D J 1973 *J. Phys. C: Solid State Phys.* **64** 1181
- [56] Schuch N, Cirac J I and Pérez-García D 2010 *Ann. Phys.* **325** 2153
- [57] Buerscher O 2014 *Ann. Phys.* **351** 447
- [58] Şahinoğlu M B, Williamson D, Bultinck N, Mariën M, Haegeman J, Schuch N and Verstraete F 2014 Characterizing topological order with matrix product operators arXiv:1409.2150
- [59] Schuch N, Poilblanc D, Cirac J I and Pérez-García D 2013 *Phys. Rev. Lett.* **111** 090501
- [60] Haegeman J, Zauner V, Schuch N and Verstraete F 2015 *Nat. Commun.* **6** 8284
- [61] Bais F A and Romers J C 2012 *New J. Phys.* **14** 035024
- [62] Chen J Y, Zhengfeng J, Zheng-Xin L, Yi S and Bei Z 2016 *Phys. Rev. A* **93** 012309
- [63] Zauner V, Draxler D, Vanderstraeten L, Haegeman J and Verstraete F 2014 Symmetry breaking and the geometry of reduced density matrices arXiv:1412.7642
- [64] Verstraete F, García-Ripoll J J and Cirac J I 2004 *Phys. Rev. Lett.* **93** 207204
- [65] Verstraete F, Murg V and Cirac J 2008 *Adv. Phys.* **57** 143
- [66] Haegeman J, Zauner-Stauber V, Fishman M and Verstraete F 2016 in preparation
- [67] Garnerone S, de Oliveira T R and Zanardi P 2010 *Phys. Rev. A* **81** 032336